Thin–Walled Structures 199 (2024) 111844

Contents lists available at ScienceDirect

Thin-Walled Structures

journal homepage: www.elsevier.com/locate/tws

Full length article

Welded beam-to-column steel joints: Assessment of European design rules

Jorge Conde [a,*], Fernando Freire [b], Filip Ljubinković [b], Martin Vild [c], Luís Simões da Silva [b]

[a] Universidad Politécnica de Madrid, Departamento de Física y Estructuras de Edificación, Av. Juan de Herrera, 4, Madrid 28040, Spain
[b] Department of Civil Engineering, University of Coimbra, ISISE, ARISE, Portugal
[c] Brno University of Technology, Faculty of Civil Engineering, Institute of Metal and Timber Structures, Veveri 95, Brno 602 00, Czech Republic

ARTICLE INFO

Keywords:
Welded steel joints
Column web in compression
Column web in tension
Column web in shear
FEM
Eurocode 3
Component method

ABSTRACT

Properly validated high-quality Finite Element (FE) models with experimental tests permit an accurate description of the load-deformation path and stress state of steel joints and are nowadays accepted as "experimental results". Changes to the design of welded joints in Eurocode 3 are currently proposed that affect the resistance and stiffness of the components associated with the column web panel. This paper presents an assessment of the design formulations included in the current Eurocode 3, part 1–8, and its forthcoming update in terms of stiffness and moment resistance, compared against a large parametric study of strong-axis beam-column welded joints for open sections carried out using validated sophisticated FE models. The results show that both the old and new Eurocode formulations provide a large scatter and no big differences between both methods. Additionally, the presence of axial force in the column shows a clear increase in the ratio between design resistance vs numerical resistance that, particularly in the case of transversally stiffened joints, may be unconservative.

1. Introduction

Welded beam-to-column steel joints between I or H sections are a standard solution to join steel profiles. They are used in single-sided (1S) or double-sided (2S) joint configurations, with (T) or without (U) transverse stiffeners usually aligned with the beam flanges, as shown in Fig. 1, where two positions, internal (I) story or roof (R) are introduced, and the optional stiffeners are indicated in dashed lines. The figure also introduces the cross-section notation used hereinafter.

Although welded beam-to-column steel joints are nowadays not favoured in many cases to avoid in situ welding, they provide the basis for the verification of the column web panel [1]. Fig. 2 shows the geometry, Von Mises stress, direct horizontal stress, and shear stress field contours (normalized to the beam yield strength f_{yb}) of a typical welded beam-to-column joint between an IPE200 beam and a HEB160 column, both in S235 steel, for a load level approximately corresponding to 87 % of the joint resistance (calculated according to EC3–1–8, see also Section 2.1 and Annex A) with column length $L_c = 4025.8$ mm, and clear distance between beam faces and column end $a = 1912.9$ mm (L_c and a are defined in Fig. 3). Full-penetration butt welds with no oversize are considered in the connection between the beam and column. The material properties for the beam are: yield strength $f_{yb} = 351$ MPa, tensile strength $f_{ub} = 519$ MPa; for the column: yield strength $f_{yc} = 280$ MPa and tensile strength $f_{uc} = 508$ MPa. Fig. 2 distinctly shows that the bending moment coming from the beam is mostly transferred by the beam flanges and has a local effect that is clearly visible in Fig. 2(b). Two components may be defined, corresponding to the effect of the load introduction in the column web panel: (1) the zone aligned with the beam top flange (column web in tension, hereby referred to as CWT) and (2) the zone aligned with the beam bottom flange (column web in compression, hereby referred as CWC). The horizontal shear corresponding to the two stress resultants coming from the beam flanges generates an approximately constant shear stress distribution, as shown in Fig. 2(c): component column web in shear, hereby referred to as CWS, corresponding to the zone aligned with the beam web. In summary, for an unstiffened column web panel, shear distortion is superimposed with direct tensile and compressive stresses induced by the loads introduced by the beam flanges. In the case of welded joints with transverse stiffeners (not illustrated in Fig. 2), the load introduction forces are directly taken by the transverse stiffeners and shear distortion is the dominant failure mode in the column web panel.

Since the load introduction in a welded joint is mostly transferred by the beam flanges, it is easy to identify and extract the applied forces on the boundaries of the web panel, whereas this is more complex in a bolted joint that exhibits multiple load introduction levels,

* Corresponding author.
E-mail address: jorge.conde@upm.es (J. Conde).

https://doi.org/10.1016/j.tws.2024.111844
Received 7 November 2023; Received in revised form 22 March 2024; Accepted 28 March 2024
Available online 30 March 2024

Symbols and acronyms

Latin letters

a	distance from axis of beam flange to closest column support (see also Fig. 3)
a_f	throat thickness of fillet weld joining beam flange (or stiffener) with column flange
a_w	throat thickness of fillet weld joining beam web and column flange
A_c	column cross-sectional area
A_{CWS}	column shear area defined in Eurocode 3, part 1–8 (see also Table A1)
A_{vc}	shear area defined in Eurocode 3, part 1–1.
BCW	beam-column weld component
BFC	beam flange and web in compression component
b_{eff}	effective width (see also Table A1)
b_{fb}	width of beam flange (see also Fig. 1)
b_{fc}	width of column flange (see also Fig. 1)
b_{st}	total width of stiffeners (see also Fig. 1)
C_1	auxiliary coefficient for the QUAD material model
CFB	column flange in bending component
CWC	column web in compression component
CWS	column web in shear component
CWT	column web in tension component
d	horizontal displacement of beam flange centroid (see also Fig. 9)
d_b	depth of beam web flat (see also Fig. 1)
d_c	depth of column web flat (see also Fig. 1)
d_{RJ}	displacement obtained assuming the joint as infinitely rigid
E	Young's modulus of steel
EN	current Eurocode 3, Part 1–8 (EN 1993–1–8:2005) [15]
EPPL	elastic-perfectly plastic material model
E_{sh}	tangent modulus of steel at onset of strain hardening
f_y	yield stress of steel
f_{yb}	yield stress of beam material
f_{yc}	yield stress of column material
f_{yst}	yield stress of stiffener material
f_u	tensile strength of steel
f_{ub}	tensile strength of beam material
f_{uc}	tensile strength of column material
F	force applied at the tip of the beam
F_b	resultant force on beam flange centroid
FprEN	upcoming Eurocode 3, Part 1–8 (FprEN 1993–1–8:2023) [22]
$f_{C1\varepsilon u}$	stress at a strain $C_1 \cdot \varepsilon_u$
G	shear modulus of steel
GMNIA	geometrically and materially nonlinear static analysis with imperfections
h_b	beam depth (see also Fig. 1)
h_c	column depth (see also Fig. 1)
h_{ib}	distance between inner faces of beam flanges (see also Fig. 1)
h_{ic}	distance between inner faces of column flanges (see also Fig. 1)
I_y	second moment of inertia of column cross-section about its strong axis
k	component stiffness
k_{wc}	reduction factor for axial force interaction
LBA	linear buckling analysis
L_b	length of beam
L_c	length of column (see also Fig. 3)
M	bending moment applied on the beam (see also Fig. 1)
M_j	bending moment applied at the joint
$M_{pl,fc,Rd}$	plastic moment resistance of column flange (see Table A1)
$M_{pl,fb,Rd}$	plastic moment resistance of beam flange (see Table A1)
M_R	moment resistance of the joint
M_{Rd}	design moment resistance of the joint
m_r	ratio between moments applied at both sides of joint (see also Fig. 3)
$M_{y,wp}$	yield moment of panel zone of column
N	column axial force (see also Fig. 3)
N_V	vertical (gravitational) force applied at column top
n	column axial force ratio
n_c	number of sides of joint (1 or 2) (see Table A1)
$N_{pl,Rk}$	plastic axial resistance of column
QUAD	Yun-Gardner quad-linear material model [26]
R	rotation degree of freedom
r	ratio between moment resistances derived with two different methods
r_b	root radius of beam (see also Fig. 1)
r_c	root radius of column (see also Fig. 1)
s	ratio between rotational stiffnesses derived with two different methods
S_j	rotational stiffness of the joint
$S_{j,ini}$	initial rotational stiffness of the joint
$S_{j,sec}$	secant rotational stiffness of the joint
t_{fb}	beam flange thickness (see also Fig. 1)
t_{fc}	column flange thickness (see also Fig. 1)
t_{st}	stiffener thickness (see also Fig. 1)
t_{wb}	beam web thickness (see also Fig. 1)
t_{wc}	column web thickness (see also Fig. 1)
U	displacement degree of freedom
V	shear force applied on the joint (see also Fig. 1)
$V_{wp,add,Rd}$	column shear resistance due to contribution of column flange and stiffeners
$V_{wp,Rd}$	column shear resistance due to contribution of column web panel
$V_{wp,tot,Rd}$	column shear resistance including all contributions (see Table A1)
$W_{pl,b}$	beam cross-section plastic modulus
z_b	distance between centroids of beam flanges (see also Fig. 1)

Greek letters

β	transformation parameter for joint shear resistance including model corrections
β_1,β_2	transformation parameter for joint shear resistance, side 1 or 2 (see also Table A1)
γ_{M0}	partial factor for cross-sectional resistance
γ_{M1}	partial factor for instability
γ_{M2}	partial factor for cross sectional tension fracture
δ	displacement at the beam tip
ε	strain
$\varepsilon_{pl,eq}$	equivalent (Von Mises) plastic strain
ε_{sh}	strain value at onset of strain hardening
ε_T	true strain
ε_u	strain value at tensile strength
ε_y	yield strain
$\bar{\lambda}_p$	column web panel notional slenderness
ν	Poisson's ratio
ρ	column web buckling reduction factor
σ	stress
$\sigma_{com,Ed}$	axial compressive stress in column web adjacent to root radius (see also Table A1)
σ_{VM}	equivalent (Von Mises) stress
σ_T	true stress
ϕ_j	joint rotation
ϕ_{jap}	apparent joint rotation (referred to the global reference system)

$\phi_{y,wp}$	yield distortion of panel zone of column		panel (see also Table A1)
ω	reduction factor for shear interaction in the column web	ω_1,ω_2	auxiliary values to calculate ω (see also Table A1)

corresponding to the various bolt rows in tension [2]. Additionally, in the case of welded joints with transverse stiffeners, shear distortion is the dominant failure mode in the column web panel. In contrast, for an unstiffened column web panel, shear distortion is superimposed with direct tensile and compressive stresses induced by the loads introduced by the beam flanges.

The behaviour of the web panel in welded joints has been the object of many studies since the early 1970s [3]. Historically, the study of welded joints with transverse stiffeners was addressed in North America and Japan through comprehensive experimental and theoretical studies [4–6] that led to: (i) the identification of the main parameters that influence the behaviour of welded joints; (ii) the importance of considering the real stress distribution and stress interactions in the column web panel; and (iii) the relevance of the vertical normal stresses to the shear resistance of the web panel. These studies led to the proposal of analytical multi-linear models for shear resistance of the web panel [7] that were incorporated in the AISC code [8] for transversely stiffened beam-to-column welded joints.

In Europe, unstiffened beam-to-column welded joints were addressed, focussing on the effects of load introduction and the corresponding stress interactions [9]. Extensive experimental test programs were carried out at the University of Innsbruck [10], complemented by numerical studies [11] that led to proposals of multi-linear analytical models for shear and load introduction [12–14] that were subsequently incorporated in Eurocode 3, part 1–8 [15], hereinafter referred to as EC3–1–8. It was concluded that the stress interactions related to the resistance of the column web panel in shear and the load introduction components could be simplified by neglecting the horizontal normal stresses for the column web panel in shear and the vertical normal stresses coming from the column for the load introduction components, for applied loads below 70 % of the plastic resistance of the column.

Based on full-scale experimental tests and calibrated numerical models, an analytical model in line with the component method was proposed for internal asymmetric joints [3]. The proposed mechanical model required the subdivision of the web panel into sub-panels and the consideration of different levels of shear for each sub-panel to address the complex stress fields in the column web panel.

High strength steel (HSS) welded joints were studied by Jordão et al. [16], who carried out experimental tests on welded joints in S690 to extend the design rules to HSS. It was concluded that the code provisions of the EC3–1–8 formulation for the resistance and stiffness of the web panel components in the case of high strength steel were too penalizing and parameters that need to be updated for HSS and welded cross sections were identified. Girão Coelho et al. [17] carried out experimental tests on web shear panels in steel grades S690 and S960, concluding that HSS web panels in shear can exhibit ductile behaviour and satisfy very high deformation demands, depending on the web slenderness, which ultimately determines the failure mode; it was also concluded that the influence of the axial force in the column over the high strength steel panel zone requires a deeper study. Recently, Corman, [18], Corman, et al. [19,20], and Jaspart et al. [21] have reassessed the behaviour of the column web panel concluding that the design expressions for the column web panel in shear were unsafe and proposed an improved formulation for the design that was included in the updated version of Eurocode 3 part 1–8 that will be subject to formal vote [22], hereinafter referred to as FprEC3–1–8.

It is the objective of this paper to assess the behaviour of welded beam-to-column steel joints, with particular emphasis on the column

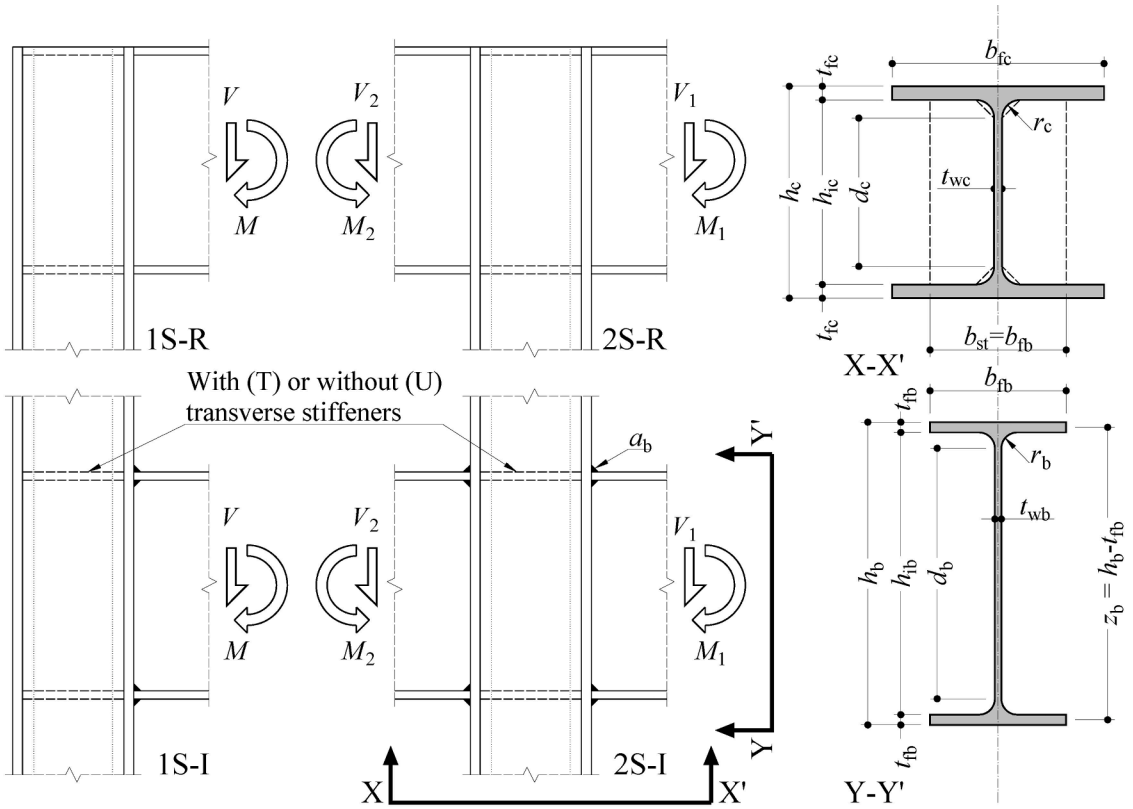

Fig. 1. Definition of cases and notation.

web panel, covering single-sided and double-sided configurations, intermediate or top floor, transversely unstiffened or stiffened, and with various levels of axial load in the column. Firstly, a sophisticated nonlinear finite element model is implemented and calibrated with experimental test results. Secondly, a large parametric study for three different steel grades is carried out. Subsequently, the observed physical phenomena are critically discussed and compared to the Eurocode design rules.

2. Materials and methods

The assessment of the Eurocode 3–1–8 design rules for welded beam-to-column steel joints is carried out by comparing the design rules available in EC3–1–8 and the forthcoming revised version FprEC3–1–8 with the results of advanced numerical simulations using FEM that follow the framework of prEN 1993–1–14 [23].

In this section, firstly, the component method and the corresponding design rules in EC3–1–8 and FprEC3–1–8 are briefly summarised. Secondly, the finite element model used in the parametric studies is described and validated. Finally, the numerical study is described, comprising the definition of the scope, the assumptions and boundaries of the study, the analysis options, and the post-processing options for the interpretation of the results.

2.1. Component model and Eurocode expressions

The component method (CM) is a well-established general procedure to determine the main structural properties (resistance and stiffness) of a joint [24]. The method is based on the identification of the joint active components, subsequent assessment of their individual structural properties, and creation of a joint model assembling the individual components by means of rigid links and springs. A detailed explanation of the CM is given in [1]. EC3–1–8 presents CM-based expressions for strong−axis open−section welded beam−column joints. According to the code, the joint resistance is limited by the most restrictive of the following individual components: column web panel in shear (CWS), column web in transverse compression (CWC), column web in transverse tension (CWT), column flange in transverse bending (CFB), beam flange and web in compression (BFC), or beam−column welds (BCW). The joint stiffness depends on the individual stiffnesses of the CWS, CWT, and CWC. Concerning joint stiffness, the CWC and CWT components can be disregarded in the presence of a transverse stiffener, aligned with the beam flange, in the compression or tension zone, respectively. The transverse stiffeners, together with the column flanges, increase the resistance of the CWS component through Vierendeel frame action. The joint is divided into a panel zone and either one (one-sided joint) or two (two-sided joint) connections. For a two-sided joint, the demand on the CWS component depends on the bending moments applied on both sides. This may be considered in a simplified manner using a transformation parameter β, which depends on the bending moment ratio between both connections. FprEC3–1–8 is based on a similar rationale but includes some adjustments based on recent numerical studies [19,20]. The geometrical notation is introduced in Fig. 1.

The EC3–1–8 and FprEC3–1–8 design expressions are summarized and compared in Table A.1 (Annex A). A concise explanation of the CM philosophy is given in Annex A. Besides the extension in FprEC3–1–8 to steel grades up to S700, the main differences between both codes are: i) the definition of the column shear area A_{CWS} (CWS); ii) the contribution of the column flange and transverse stiffeners (CWS) in strength; iii) the definition of the web panel slenderness and buckling expressions (CWC). Using the expressions in the Annex, where the resistances of individual components are multiplied by the lever arm z_b, the values of moment resistance limited by the joint components as per EC3–1–8 are: $M_{CWS,R,EN}$, $M_{CWC,R,EN}$, $M_{CWT,R,EN}$, $M_{CFB,R,EN}$, $M_{BCW,R,EN}$. The moment resistance of the joint (referred to as the moment applied on side 1), is assessed as follows:

$$M_{R,EN} = \min\left\{M_{CWS,R,EN}; M_{CWC,R,EN}; M_{CWT,R,EN}; M_{CFB,R,EN}; M_{BCW,R,EN}\right\} \quad (1)$$

The joint initial stiffness defined by EC3–1–8 and referred to as joint 1 can be obtained from the stiffness of the components $k_{CWS,EN}$, $k_{CWC,EN}$, $k_{CWT,EN}$, as:

$$S_{j,ini,EN} = E\, z_b^2 \left(k_{CWS,EN}^{-1} + k_{CWC,EN}^{-1} + k_{CWT,EN}^{-1}\right)^{-1}, \quad (2)$$

and the secant stiffness $S_{j,sec,EN}$ is 1/3 of the initial stiffness. Eqs. (1) and (2) can be used for $M_{R,FprEN}$, $S_{j,ini,FprEN}$, and $S_{j,sec,FprEN}$, replacing the EN components by those obtained with the FprEC3–1–8 expressions ($M_{CWS,R,FprEN}$, $M_{CWC,R,FprEN}$, $M_{CWT,R,FprEN}$, $M_{CFB,R,FprEN}$, $M_{BCW,R,FprEN}$, $k_{CWS,FprEN}$, $k_{CWC,FprEN}$, $k_{CWT,FprEN}$).

2.2. Finite element models

2.2.1. Description of the models

Detailed numerical models are developed using the commercial FE software Abaqus [25], following the requirements and recommendations given in the forthcoming prEN 1993–1–14 [23]. Geometrically and materially nonlinear static analysis with initial imperfections (GMNIA) is chosen to reproduce the real behaviour of welded joints. The FE solid model comprises a solid core region connected to shell parts using solid-shell couplings. The length of the members within the solid core part is defined as 1.25 times the depth of the member on each side,

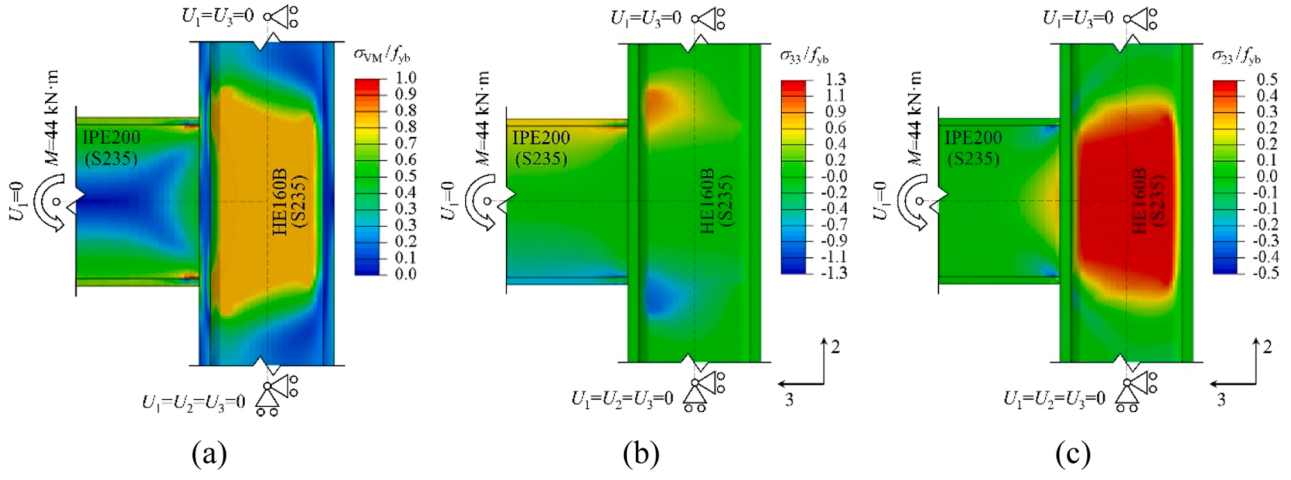

Fig. 2. Normalized stress field contours of a typical one-sided welded joint: (a) Von Mises stress field; (b) direct horizontal (3–3) stress; (c) shear (2–3) stress.

measured from the joint face. Fig. 3 presents a conceptualization of the model, adapted to the four joint configurations analysed in this study.

Considering the computational time and storage required per model and the large size of the parametric study, different element types are tested, and an eight-node linear brick element with reduced integration (C3D8R) is selected to model the solid core. Likewise, the shell parts are modelled using four-node linear shell elements with reduced integration (S4R). For the sake of simplicity, the beam root radius zone is not modelled, resulting in a small reduction of the beam moment resistance. Full penetration butt welds are considered in the connection between the beam and the column, resulting in some nuances which are further discussed below. Additionally, in the joints with transverse stiffeners, these are assumed of equal width and thickness as the beam flange, but with the same material as the column, and full penetration butt welds are assumed between the stiffener and the column. The steel material is considered using nominal material properties. Two alternatives are considered: (i) an elastic-perfectly plastic material (EPPL) with no strain hardening; and (ii) the quad-linear material model developed by Yun and Gardner [26] that considers strain hardening. Young's modulus of steel E and Poisson's ratio ν are taken as 210 GPa and 0.3, respectively. Annex B summarizes the constitutive laws for both materials.

The nodes at the extremities of the column and beams are constrained to the motion of a reference point through rigid-body constraints. The boundary conditions used in the analysis are shown in Fig. 3. The load is introduced through a bending moment $M_1 = M$ applied at the tip of beam 1 and, for 2S joints, an additional bending moment $M_2 = m_r \cdot M$ at the tip of beam 2. For joints at an internal story (I), the axial load N, if included, is applied as a concentrated vertical force $N_V = N$ on the top node of the column.

A mesh sensitivity analysis is performed, in which the mesh is progressively refined until no significant variation is observed on the moment-rotation curve. At least four elements are placed across the

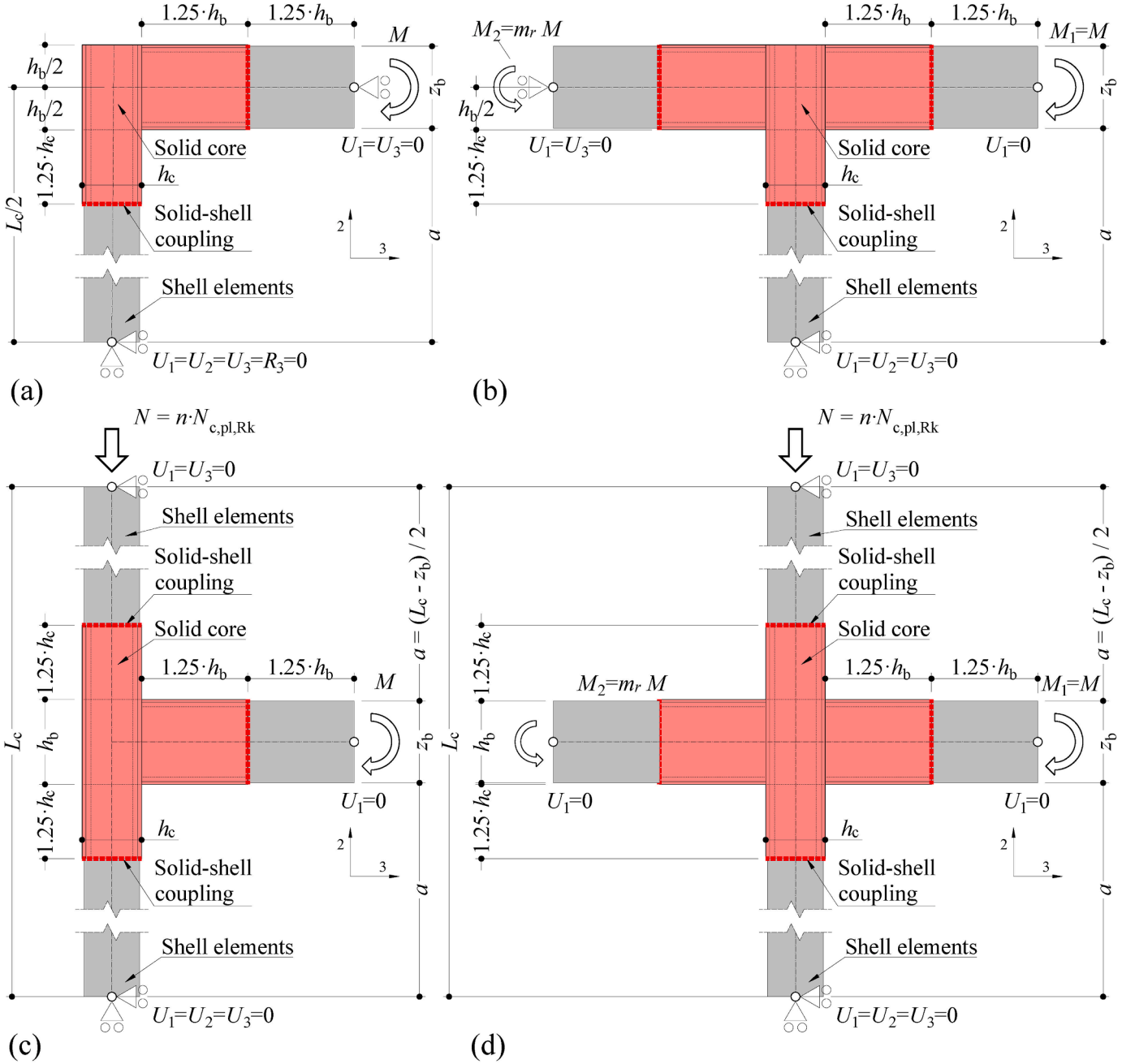

Fig. 3. Layout for FE models: (a) 1S-R; (b) 2S-R; (c) 1S-I; (d) 2S-I.

thickness of all plates in the solid core. For the region with larger stress variations (intersection between the beam and the column), a finer mesh is employed. This "refined region" extends up to $0.3h_b$ in the beam and $0.6h_c$ in the column, see Fig. 4. The mesh is also optimized at the cross-section level, where regions with stress concentrations are more refined, e.g., close to the root radius. The worst and average aspect ratios of the elements are also controlled and kept below 3 (average) and 6 (worst).

Initial geometric imperfections are introduced in the FE solid models by considering the first buckling mode from a linear buckling analysis (LBA), with an amplitude of $d_c/200$. For some models, an initial amplitude of $d_c/420$ is also examined that corresponds to the equivalent geometric imperfection that matches the Winter curves [27]. Residual stresses are not explicitly modelled. For the LBA, only the web panel is free to move in the out-of-plane direction, to avoid spurious modes, and no axial force is applied to the column. Fig. 5 depicts examples of initial imperfections obtained for different joint layouts.

The numerical models are generated, run, and monitored automatically through Python scripts. The analysis is stopped when the maximum equivalent plastic strain $\varepsilon_{pl,eq,max}$ on the solid core reaches about 10 %, or when instability is reached. The 10 % value for $\varepsilon_{pl,eq,max}$ is twice the generic reference value (5 %) for tolerable strain included in the current draft of Eurocode 3 part 1–14 (prEN1993–1–14) [23], and ensures that this criterion is reached during the analysis. Results of the analysis include stress, strain, displacement components from the web panel, and reactions. These are obtained both in numerical and graphical formats. Joint rotations are derived from displacements as explained below.

Further explanation is needed regarding the weld resistance. As mentioned, welds are not modelled in this study and are assumed to be full penetration butt welds, with no oversize. Hence, overmatching welds are assumed. The critical fusion face is assumed to be located at the interface of the beam in contact with the column. The moment resistance of the joint is limited by the moment resistance of the beam-column contact, calculated using the mechanical properties of the weakest material, either beam or column, as stated in Section 4.7.1 of EC3–1–8 or Section 6.7.1 of FprEC3–1–8. This failure mode, however, would require a much more sophisticated FE model in the weld zone to be properly captured for the following reasons. Firstly, proper consideration of the material properties in the fusion zone and the heat-affected zone would have to be considered, with a much more refined mesh and fracture models such as, e.g., the Johnson-Cook model [28]. Secondly, consider a joint in which the column material is weaker than the beam material. In the corresponding FE model, focusing on a solid finite element that belongs to the column, and is located at the interface between the column and the beam, four nodes (A, B, C, D) define the outermost face of the element that is in contact with the beam, and four additional nodes (E, F, G, H) define the innermost face of the same element. The integration point (I) is located at the Gauss point, within the boundaries of the surface defined by these eight nodes. Due to the large dispersion of stress across the thickness of the column flanges, the stresses at the innermost face will be much lower than those on the outermost face. However, the stress and strain values are unique for the element and are calculated at the integration point, which defines the stress-strain behaviour of the whole element. Thus, the interface between the beam and the column might present very different values of normal stress, depending on which elements (beam or column) are selected. The models for which this phenomenon happens are easily detected, as those for which the FEM moment resistance is larger than the plastic moment resistance calculated by multiplying the strong-axis plastic modulus of the beam $W_{pl,b}$ by the weakest of the yield strength of the beam or column $\min\{f_{yc}, f_{yb}\}$. The failure mode for these models is weld failure and they are disregarded in the assessment.

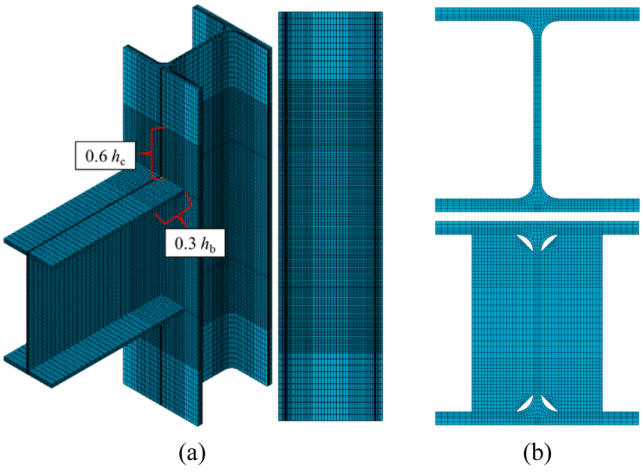

Fig. 4. FE mesh for the solid core: (a) Refined region; (b) Cross section – unstiffened and stiffened.

2.2.2. Validation of models

The FE solid model is validated against the experimental results of two welded joints in S235 studied by Klein [29] and three welded joints in S355 studied by Jordão [30]. The joints are subjected to bending moment, with no axial load in the column. Table 1 presents the geometrical properties of the selected joints. For tests NR4 and NR16, only the yield strength f_y and tensile strength f_u were made available in [29]. In these cases, the quad-linear material model from prEN 1993–1–14 [23] is used to build the stress-strain curves for each plate. The measured material properties for tests E1.1, E1.2, and E2, reported in [30], are used in the models. Pinned boundary conditions are applied to the column ends, and the out-of-plane displacement is restrained at the beam end. A vertical displacement is introduced on the tip of the beam to simulate the real loading conditions. The initial imperfections are accounted for by considering the first buckling mode from an LBA, with an amplitude of $d_c/200$.

Fig. 6 presents a comparison between the experimental ("Exp") and the numerical ("Num") results for the Klein tests. The load-deflection curves correlate the vertical displacement at the tip of the beam (δ) and the applied vertical force (F). Numerical and experimental results present a very good match. Fig. 7 presents similar results for the Jordão tests, using the applied bending moment M. For the double-sided joint S355 E2, the labels "SB" and "LB" refer to small beam and large beam, respectively. For each joint, the final deformed shape obtained in the experimental test is compared with the corresponding one obtained from the numerical model. The comparisons show that there is a good agreement between experimental and numerical results in terms of initial stiffness, resistance, and deformation. The largest differences in the $M-\delta$ curves are obtained for test S355 E2. However, it can be stated that the overall behaviour of the joint is well captured, given the uncertainties from the experimental test. Therefore, the FE solid model is successfully validated using experimental data available in the literature, meaning that the developed model provides a powerful tool for conducting extensive parametric studies.

2.3. Numerical study

2.3.1. Scope of study and case selection

The objective of the study is to confront the FEM results with the predictions of EC3–1–8 [15] and FprEC3–1–8 [22] for a large and representative sample of beam−column joints, to assess the accuracy of the code expressions. Fig. 1 introduced the four different joint layouts treated: single-sided for internal story (1S-I) or roof (1S-R), and double-sided for internal story (2S-I) or roof (2S-R). Stiffened configurations for all layouts are considered and referred to with the tag 'T'. Unstiffened layouts are untagged or tagged as 'U'. The study presents the following scope and limitations: i) only welded joints are considered; ii) only European hot−rolled, open−sections are assumed; (iii) the

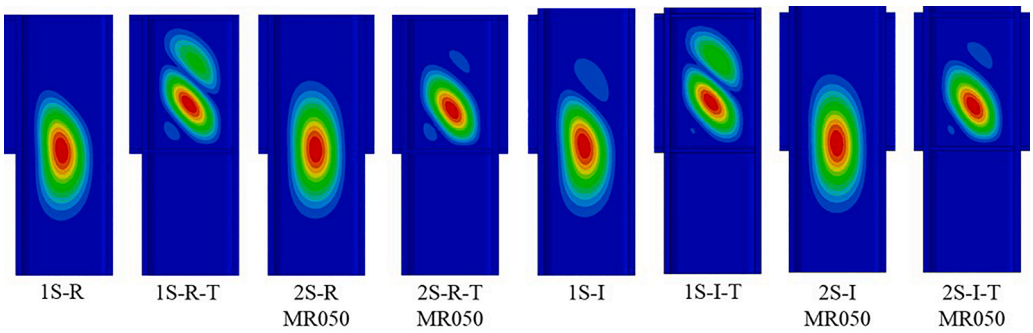

Fig. 5. Initial geometric imperfections for FE solid models.

Table 1
Geometry of the selected welded joints for validation.

Author	Test	Member	h_c, h_b(mm)	b_{fc}, b_{fb}(mm)	t_{wc}, t_{wb}(mm)	t_{fc}, t_{fb}(mm)	r_c, r_b(mm)	L_c, L_b(mm)	a_f(mm)	a_w(mm)
Klein (1985)	S235 NR4	Col HEB160	159.0	160.0	8.0	12.2	15	1350	7.1	–
		Beam IPE330	329.0	162.0	8.0	11.4	18	698		
	S235 NR16	Col HEB300	298.0	300.0	10.6	18.0	27	1600	12.7	–
		Beam HEB500	500.0	301.0	14.7	27.6	27	580		
Jordão (2008)	S355 E1.1	Col HEB240	245.4	242.3	10.4	16.5	21	3000	16.0	0.0
		Beam IPE400	404.3	179.5	8.8	12.8	21	1300		
	S355 E1.2	Col HEB240	246.0	241.4	10.6	16.8	21	3000	16.0	5.0
		Beam IPE400	406.8	179.1	9.1	13.1	21	1300		
	S355 E2	Col HEB240	245.6	241.3	10.3	16.5	21	3000	0.0	0.0
		Beam1 IPE400	402.7	178.8	8.9	12.9	21	1300	16.0	5.0
		Beam2 HEB200	199.0	201.0	9.0	14.4	18	700	13.0	6.0

No information available: "-".

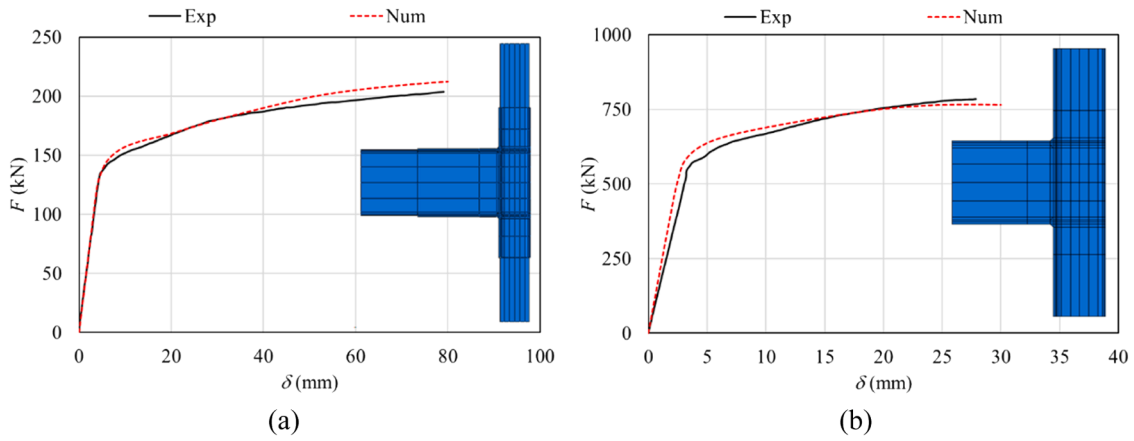

Fig. 6. Experimental vs numerical results for tests from Klein [29]: (a) NR4; (b) NR16.

following steel grades, S235, S275, and S355 are addressed; iv) only strong−axis joints, with no weak−axis interaction, are considered; v) for stiffened joints, transverse stiffeners are placed in both tension and compression areas simultaneously; vi) full-penetration butt welds between the beam and the column are assumed and they are not modelled, considering perfect continuity between the welded parts; and vii) several levels of axial load for the column (0 %, 30 %, 50 %, 70 % of the column section plastic resistance) are considered.

The features of the FE models used in the study and their validation have already been discussed in the previous section. The layout, loading, and boundary conditions for the different models (1S-I, 1S-R, 2S-I, 2S-R) are presented in Fig. 3. The moment M_1 is always the largest, that is, $-1 \leq m_r = M_2/M_1 < 1$, where m_r is the ratio between the applied moments at side 1 and 2, taken as 0 for the single-sided configurations. As discussed, the models present a 'solid core' which is the focus of the study.

The response of the joint is expected to depend on the column web panel slenderness d_c/t_{wc}, the column shear area A_{vc}, and the aspect ratio of the panel z_b/d_c. The selection of cases (defined as a combination of column and beam) in this study is based on these parameters. To select columns based on current engineering practice, the complete database of rolled sections typically used for columns in Europe (HE and UC, excluding large columns with $h_c \geq 600$ mm), is placed in the $(A_{vc}) - (d_c/t_{wc})$ space, which is then divided into 5 parts by 4 horizontal lines located at chosen values of d_c/t_{wc}, so that each part contains 1/5 of the total number of columns. The process is repeated for the vertical axis. The space is thus divided into 25 quadrants. 5 columns are then selected from 5 different quadrants following the Latin hypercube methodology, whereupon each column belongs to a different vertical and horizontal partition than the rest. Additionally, 2 large columns ($h_c \geq 600$ mm) are then included in the sample. In the selection of the 7 columns, care has been taken to choose a variety of cross-section types, including HEA,

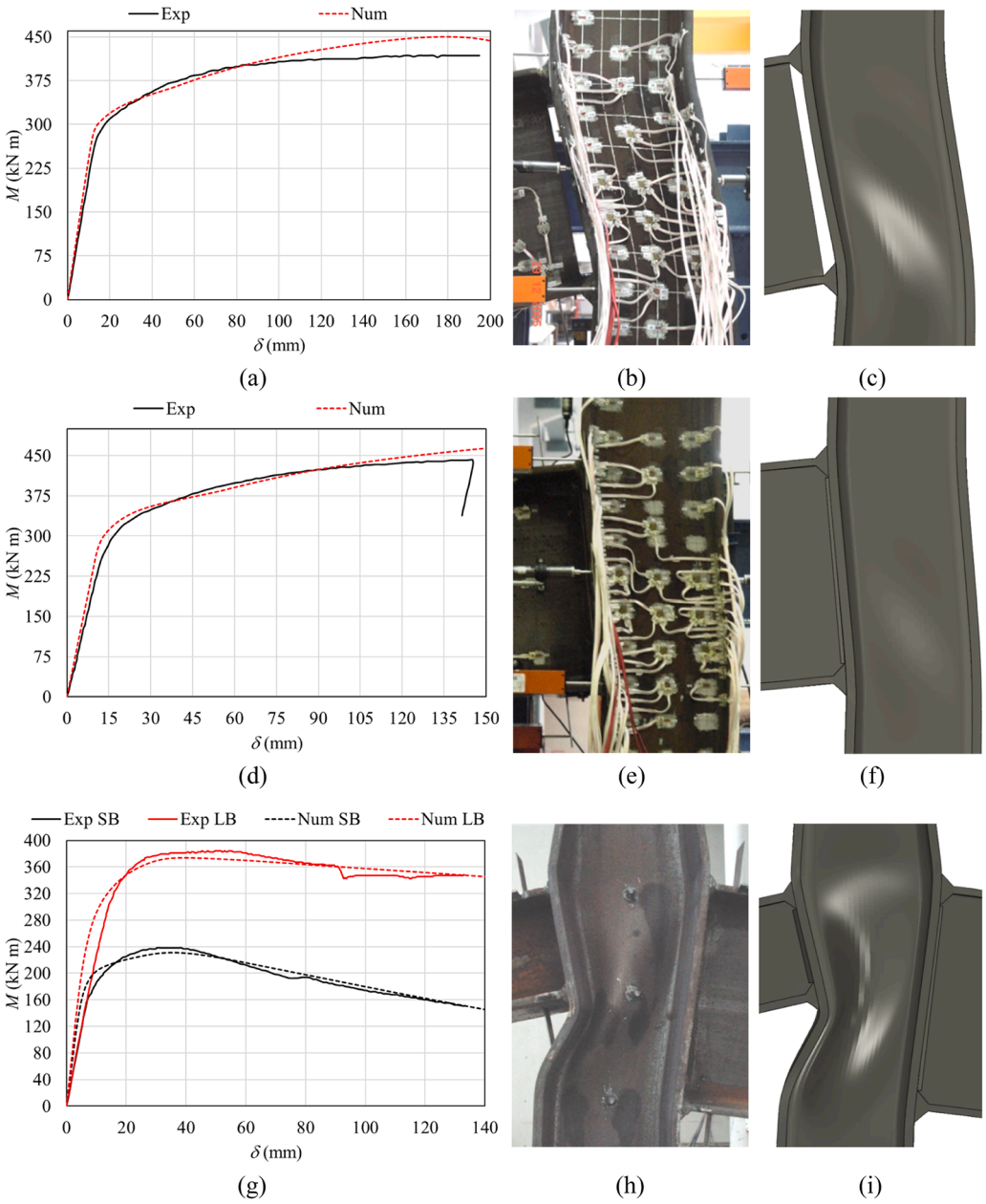

Fig. 7. Experimental vs numerical results for tests from Jordão [30].
Test E1.1: (a) *M*-*δ* curves; (b) specimen deformation at test end; (c) FEM deformation at test end.
Test E1.2: (d) *M*-*δ* curves; (e) specimen deformation at test end; (f) FEM deformation at test end.
Test E2: (g) *M*-*δ* curves; (h) specimen deformation at test end; (i) FEM deformation at test end.

HEB, HEM, and UC profiles. The points defining the final column selection in the $(A_{vc}) - (d_c/t_{wc})$ space are displayed in Fig. 8. To complete the case definition, 3 European beams (from the pool of IPE, HE, UC, UB) are individually selected for each column, providing panel aspect ratios of approximately 1, 1.5 and 2. The aspect ratio of 2 was not possible for column HE800B, therefore a total of 20 cases ($3 \times 6 + 2 \times 1$) are defined and listed in Table 2. The beam profile and steel grade are selected using two criteria: i) the beam must be quasi-elastic at the loading step where the joint moment resistance is reached, and ii) the beam must fulfil the requirements of EC3–1–8 (see clause 4.10(3) in the code) for unstiffened joints. The panel zone yield moment $M_{y,wp}$ and yielding distortion $\phi_{y,wp}$ are defined as follows:

$$M_{y,wp} = z_b\, h_c\, t_{wc} f_{yc} \Big/ \sqrt{3}, \tag{3}$$

$$\phi_{y,wp} = f_{yc} \Big/ \left(G\sqrt{3}\right). \tag{4}$$

The yield distortion only depends on the steel grade while the panel zone yield moment also depends on the geometry of the column cross-section and is included in Table 2. Both parameters will be later used to normalize the FEM results.

The study is divided into sets. Every set comprises the 20 cases defined in Table 2, but with differences in i) sides (one-sided '1S', two-sided '2S'); ii) joint location (internal story 'I', roof 'R'); iii) use ('T') or not ('' or 'U') of transverse stiffeners; iv) level of axial force ($n = 0$ %, 30 %, 50 % or 70 %, as a ratio between the applied axial load and the characteristic column axial load resistance $N_{pl,Rk} = A_c{\cdot}f_{yc}$, where f_{yc} is the column yield strength); v) for two-sided joints only, moment ratio between both sides ($m_r = M_1/M_2 = 0.50, -0.50, -1.00$). The one-sided joint can be considered as a special case of the two-sided joint with $m_r =$

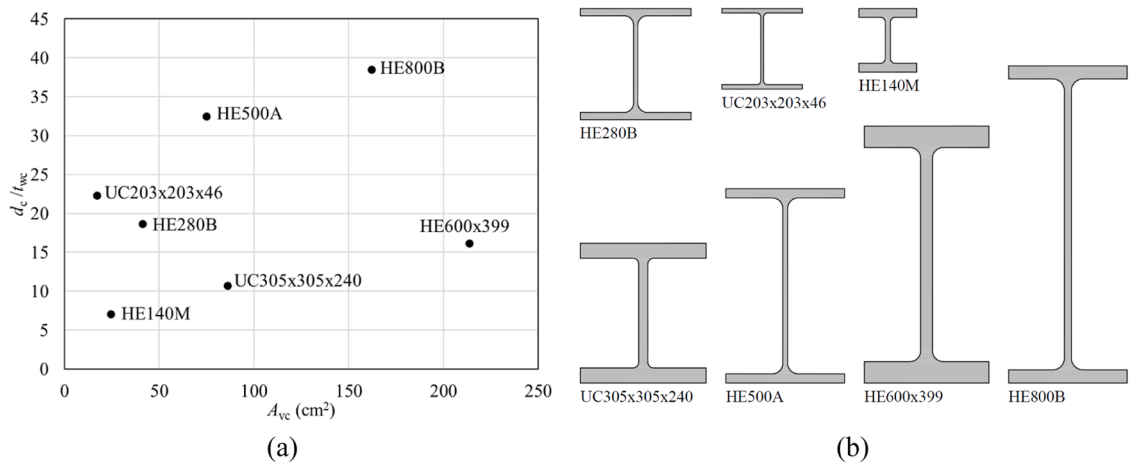

Fig. 8. Selection of columns: (a) situation in the (A_{vc}) – (d_c/t_{wc}) space; (b) column cross-sections.

Table 2
Cases included in each set.

n	Column	Beam	d_c/t_{wc}	h_b/d_c	L_c (mm)	$M_{y,wp}$ (kNm)		
						S235	S275	S355
01	HE500A	HE400B	32.50	1.03	3400	300.0	351.0	453.1
02	HE500A	HE600A	32.50	1.51	3590	450.7	527.5	680.9
03	HE500A	HE800B	32.50	2.05	3800	611.9	716.1	924.4
04	UC203 × 203 × 46	HE160A	22.39	0.94	3152	28.4	33.2	42.9
05	UC203 × 203 × 46	IPE240	22.39	1.49	3240	45.7	53.5	69.0
06	UC203 × 203 × 46	IPE330	22.39	2.05	3330	63.2	74.0	95.5
07	HE280B	HE200B	18.67	1.02	3200	73.8	86.4	111.5
08	HE280B	IPE300	18.67	1.53	3300	115.4	135.0	174.3
09	HE280B	IPE400	18.67	2.04	3400	154.2	180.4	232.9
10	HE140M	HE100B	7.08	1.09	3100	25.4	29.7	38.4
11	HE140M	HE140B	7.08	1.52	3140	36.1	42.3	54.6
12	HE140M	IPE200	7.08	2.17	3200	54.0	63.2	81.6
13	UC305 × 305 × 240	HE260B	10.31	1.10	3260	266.8	312.2	403.0
14	UC305 × 305 × 240	HE360B	10.31	1.52	3360	371.3	434.4	560.8
15	UC305 × 305 × 240	IPE500	10.31	2.11	3500	532.4	623.0	804.3
16	HE600 × 399	HE450M	16.20	0.98	4478	1155.3	1351.9	1745.2
17	HE600 × 399	HE700M	16.20	1.47	4716	1783.0	2086.5	2693.5
18	HE600 × 399	HE1000M	16.20	2.07	5008	2553.2	2987.7	3856.9
19	HE800B	HE700B	38.51	1.04	4700	1268.9	1484.8	1916.8
20	HE800B	HE1000B	38.51	1.48	5000	1831.1	2142.8	2766.1

0. The 40 sets thus defined are listed in Table 3, leading to a total of 800 models. Furthermore, the same 40 sets are defined for three different steel grades of the column (S235 with f_{yc} = 235 MPa, S275 with f_{yc} = 275 MPa; and S355 with f_{yc} = 355 MPa), thus totalling 2400 high-quality numerical models. The steel grade name precedes the set name listed in Table 3 (for example, S235_set_01, etc.). The influence of the material model (elastic-perfectly-plastic or strain hardening) and the amplitude of the initial imperfections (d_c/420 instead of d_c/200) is also assessed for one-sided internal joints (sets 01 to 04) in steel S275, adding 320 extra cases to the study.

2.3.2. Analysis

The FE models are subjected to increasing moments with load−controlled GMNIA. For two-sided joints, the proportion between the applied moments at both beams m_r is kept constant throughout the procedure. The analysis is ended when the maximum plastic true equivalent strain $\varepsilon_{pl,eq,max}$ at the joint solid core (beam excluded) is larger than the limit $\varepsilon_{pl,eq,lim}$ = 10 %, or when a numerical lack of convergence, indicative of physical instability, is reached.

2.3.3. Post-processing and data extraction

For this study, the relevant output variables of the FE model for each loading step, see Fig. 9(a), are: i) the applied moment $M = M_1$ (for two-sided joints $M_2 = m_r \cdot M_1$, where a positive value of m_r indicates tension at the beam top); ii) the displacements $d_{FEM,T1}$, $d_{FEM,T2}$ (top) and $d_{FEM,B1}$, $d_{FEM,B2}$ (bottom), measured as the average of the displacements of the corresponding (1 or 2) beam top (T) or bottom (B) flanges on its connected column face; iii) the maximum value of $\varepsilon_{pl,eq,max}$ in the central solid core. For a better understanding of the joint behaviour, $\varepsilon_{pl,eq.max}$ is obtained at each load step for 7 independent regions of the solid core, namely, WP (web panel), S1RR, S2RR (root radius region in column struts 1 or 2), S1FL, S2FL (flange region in column struts 1 or 2), BEAM1 and BEAM2. These solid core regions are shown in Fig. 9(b). $\varepsilon_{pl,eq,max}$ is always retrieved at the FE element integration points with no averaging.

The FE model displacements ($d_{FEM,T1}$, $d_{FEM,T2}$, $d_{FEM,B1}$, $d_{FEM,B2}$) include components due to the column flexibility. To assess only the joint behaviour, these components must be removed as follows:

$$d_{T1} = d_{FEM,T1} - d_{RJ,} \tag{5}$$

$$d_{B1} = d_{FEM,B1} + d_{RJ,} \tag{6}$$

where d_{RJ} is the analytical displacement obtained assuming that the column is infinitely rigid in the joint region. Similar equations can be written for d_{T2} and d_{B2}. d_{RJ} can be calculated as [10]:

Table 3
Sets contemplated in the study for every steel grade.

Set	Sides	Location	n	Stiffened	$m_r = M_2/M_1$
Set 01	1S	I	0 %		–
Set 02_N30	1S	I	30 %		–
Set 02_N50	1S	I	50 %		–
Set 02_N70	1S	I	70 %		–
Set 03	1S	I	0 %	T	–
Set 04_N30	1S	I	30 %	T	–
Set 04_N50	1S	I	50 %	T	–
Set 04_N70	1S	I	70 %	T	–
Set 05_MR-100	2S	I	0 %		−1
Set 05_MR-050	2S	I	0 %		−0.50
Set 05_MR050	2S	I	0 %		0.50
Set 06_N30_MR-100	2S	I	30 %		−1
Set 06_N30_MR-050	2S	I	30 %		−0.50
Set 06_N30_MR050	2S	I	30 %		0.50
Set 06_N50_MR-100	2S	I	50 %		−1
Set 06_N50_MR-050	2S	I	50 %		−0.50
Set 06_N50_MR050	2S	I	50 %		0.50
Set 06_N70_MR-100	2S	I	70 %		−1
Set 06_N70_MR-050	2S	I	70 %		−0.50
Set 06_N70_MR050	2S	I	70 %		0.50
Set 07_MR-100	2S	I	0 %	T	−1
Set 07_MR-050	2S	I	0 %	T	−0.50
Set 07_MR050	2S	I	0 %	T	0.50
Set 08_N30_MR-100	2S	I	30 %	T	−1
Set 08_N30_MR-050	2S	I	30 %	T	−0.50
Set 08_N30_MR050	2S	I	30 %	T	0.50
Set 08_N50_MR-100	2S	I	50 %	T	−1
Set 08_ N50_MR-050	2S	I	50 %	T	−0.50
Set 08_ N50_MR050	2S	I	50 %	T	0.50
Set 08_ N70_MR-100	2S	I	70 %	T	−1
Set 08_ N70_MR-050	2S	I	70 %	T	−0.50
Set 08_ N70_MR050	2S	I	70 %	T	0.50
Set 09	1S	R	0 %		–
Set 11	1S	R	0 %	T	–
Set 13_MR-100	2S	R	0 %		−1
Set 13_MR-050	2S	R	0 %		−0.50
Set 13_MR050	2S	R	0 %		0.50
Set 15_MR-100	2S	R	0 %	T	−1
Set 15_MR-050	2S	R	0 %	T	−0.50
Set 15_MR050	2S	R	0 %	T	0.50

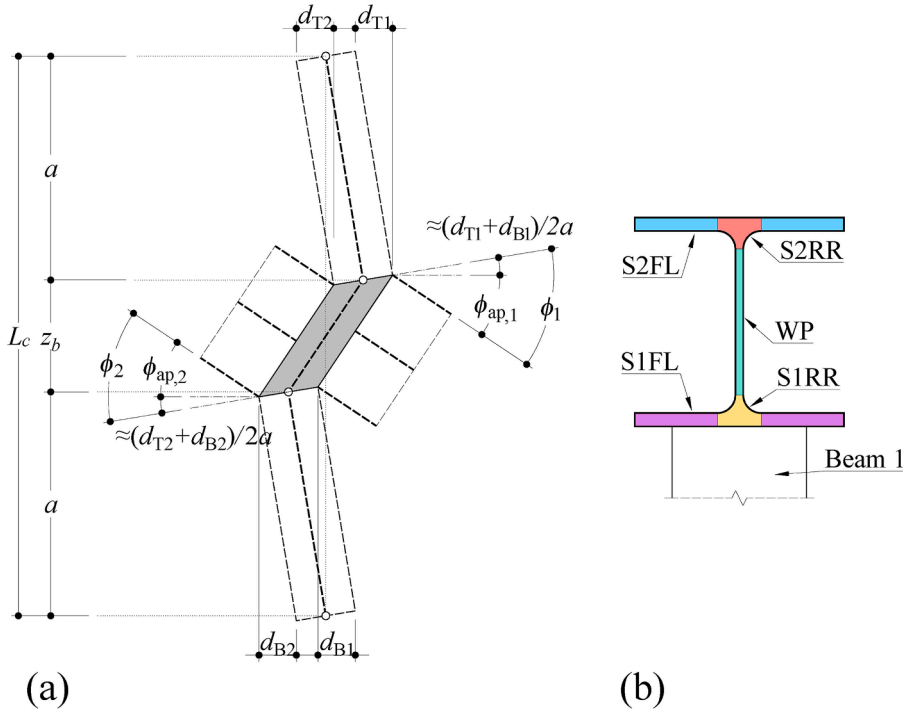

Fig. 9. Joint output: (a) kinematic variables; (b) solid core regions.

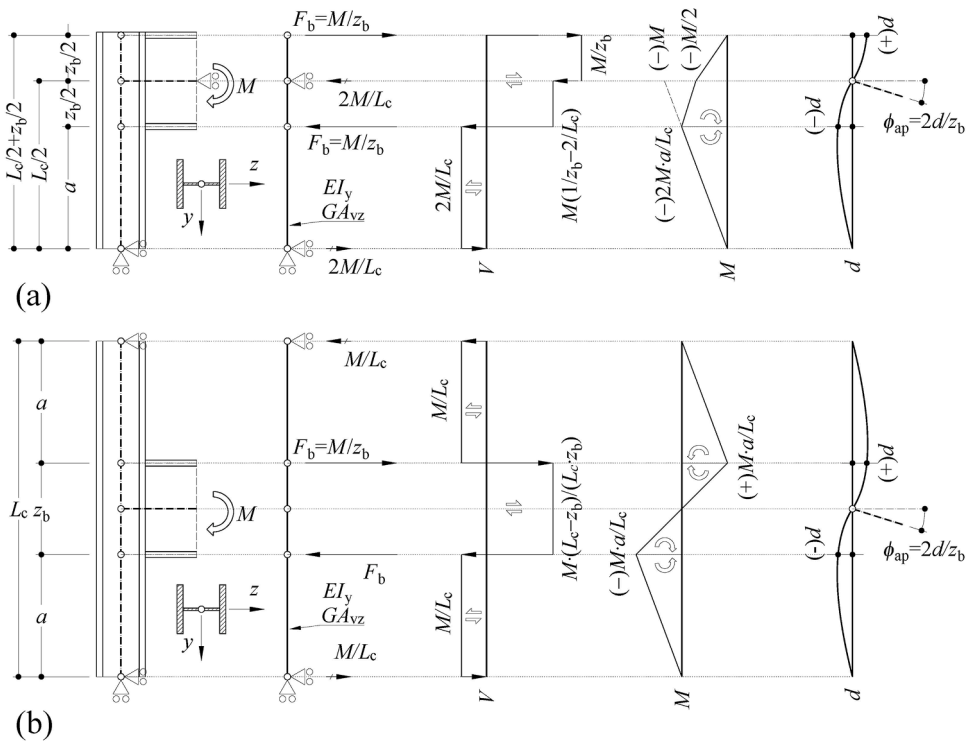

Fig. 10. Internal forces on equivalent beam models: (a) Roof joint; (b) Internal joint.

$$d_{\mathrm{RJ,I}} = M(1-m_{\mathrm{r}})\left(\frac{z_{\mathrm{b}}\,a^3}{3L_{\mathrm{c}}^2 EI_{\mathrm{y}}}+\frac{z_{\mathrm{b}}\,a}{L_{\mathrm{c}}^2 GA_{\mathrm{vc}}}\right), \tag{7}$$

$$d_{\mathrm{RJ,R}} = 2d_{\mathrm{RJ,I}}, \tag{8}$$

where $d_{\mathrm{RJ,I}}$ is the correction term corresponding to the double-sided internal story configuration (I), $d_{\mathrm{RJ,R}}$ is the correction term for the single-sided roof configuration (R), EI_{y} is the column bending stiffness, GA_{vc} is the column shear stiffness, E is the Young modulus, I_{y} is the column second moment of inertia for the strong axis, G is the steel shear modulus and A_{vc} is the column shear area coupled with I_{y}; all other variables in the expression are geometrically defined in Figs. 1 and 3. For the one−sided joint, the same expressions apply, with $m_{\mathrm{r}} = 0$. Second-order displacements are not considered because they are negligible for the structural models considered in the parametric study.

The corresponding analytical values of the design moment resistance according to EC3–1–8/FprEC3–1–8 are obtained by applying the component method, as briefly described in Section 2.1. For direct comparison with the moment resistance obtained directly from the FEM models, the moment resistance given by EC3–1–8/FprEC3–1–8 corresponding to the CWS component according to the component method, $M_{\mathrm{CWS,Rd,1}}$, is calculated using Eqs. (9) and (10) for the internal configuration, as shown by Fig. 10(b).

$$M_{\mathrm{CWS,Rd,1}} = \frac{V_{\mathrm{wp,tot,Rd}}\,z_{\mathrm{b}}}{\beta}, \tag{9}$$

$$\beta = 1 - m_{\mathrm{r}} - \frac{z_{\mathrm{b}}}{L_{\mathrm{c}}}(1+m_{\mathrm{r}}). \tag{10}$$

As seen in Figs. 9, 10(a), the corrected displacements obtained with the previous procedure define the apparent rotation $\phi_{\mathrm{j,ap}}$ (measured from the horizontal), but the total joint rotation ϕ_{j} must be measured from the column axis, by adding the term $(d_{\mathrm{T1}}+d_{\mathrm{B1}})/(2a)$, or $(d_{\mathrm{T2}}+d_{\mathrm{B2}})/(2a)$, as indicated in the figure. The joint moment−rotation (M−ϕ_{j}) curve is built in this way, and its initial rotational stiffness is calculated as $S_{\mathrm{j,ini,FEM}} = M/\phi_{\mathrm{j}}$ at the first loading step. The moment resistance $M_{\mathrm{R,FEM}}$ is obtained in an automatic way as the minimum of: i) the maximum

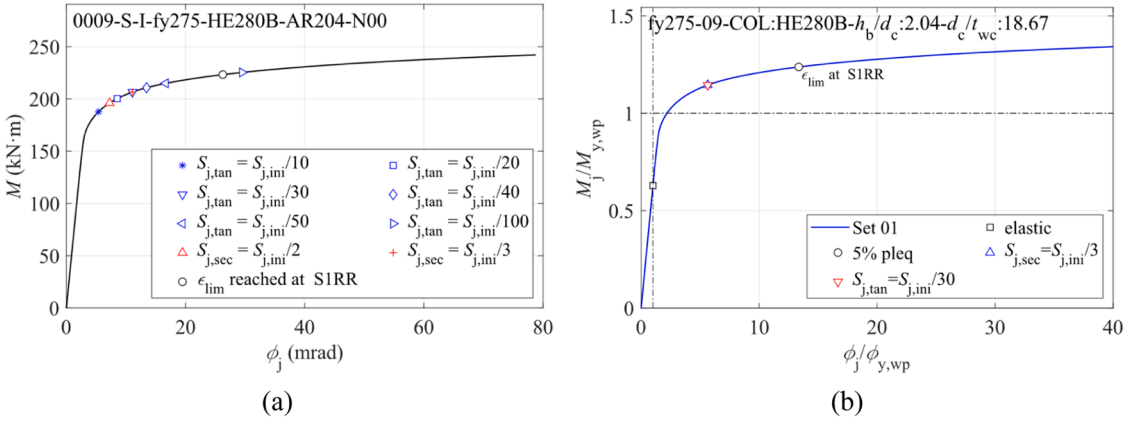

Fig. 11. Moment−rotation plots: (a) natural; (b) normalized.

value reached during analysis; ii) the moment applied at the last loading step where $\varepsilon_{pl,eq,max} \leq 5$ % (within the solid core). This criterion leads to similar results (slightly larger, on average) as the application of graphical criteria based on the intersection of the initial stiffness of the joint and the post-limit stiffness or the intersection of a secant stiffness with the moment rotation curve. The joint rotation value at this step is $\phi_{j,R,FEM}$, and the secant stiffness $S_{j,sec,FEM}$ is defined as $M_{R,FEM}/\phi_{j,R,FEM}$. For brevity, the subscript 'FEM' is removed in successive equations, plots, and tables.

To compare different cases, the FEM moment−rotation curves and the values of M_R and rotation $\phi_{j,R}$, are presented normalized to the panel zone yield moment $M_{y,wp}$ and yield distortion $\phi_{y,wp}$ using Eqs. (3) and (4). The values of $M_{y,wp}$ for the columns included in the study are listed in Table 2. The values of $\phi_{y,wp}$ are 0.168 % (S235), 0.197 % (S275), and 0.254 % (S355). An example of natural and normalized moment-rotation plots is shown in Fig. 11. In the plots, the point ε_{lim} is identified, and the column region where the limit is achieved is indicated (in the plot, S1RR). The points where different values of secant ($S_{j,sec}$) and tangent ($S_{j,tan}$) stiffness, as a ratio of the initial ($S_{j,ini}$) stiffness, are also marked. The stiffnesses values are defined numerically as follows:

- The secant stiffness at loading step k ($S_{j,sec,k}$) is determined as the ratio between the applied bending moment at step k ($M_{j,k}$) and joint rotation at step k ($\phi_{j,k}$).
- The initial stiffness ($S_{j,ini}$) is determined as the secant stiffness at the first loading step ($k = 1$).
- The tangent stiffness at loading step k ($S_{j,tan,k}$) is determined as the ratio between the increment of applied bending moment from step k to step $k + 1$ ($M_{j,k+1}$ - $M_{j,k}$), and the increment of joint rotation from step k to step $k + 1$ ($\phi_{j,k+1}$ - $\phi_{j,k}$). For the last loading step, the tangent stiffness is undefined.

2.3.4. Summary of assumptions

Besides the boundaries and limitations of the study described in Section 2.2.1, which are related to the definition of the parametric study, the finite element model and the numerical study require the adoption of some options that affect the results. Most of them lead to the underestimation of the real resistance of the welded joints (safe-sided estimates) and were already introduced in Sections 2.2 and 2.3. They are listed as follows:

- Option 1: Full penetration butt welds are considered in the connection between the beam and the column, resulting in some nuances, discussed in Section 2.2.1. Additionally, in the joints with transverse stiffeners, these are assumed of equal width, and thickness as the beam flange.
- Option 2: The steel material is modelled as elastic-perfectly plastic (EPPL) with no strain hardening. Nevertheless, the influence of strain hardening is also assessed and discussed.
- Option 3: Initial geometric imperfections are introduced in the FE solid models by considering the first buckling mode from a linear buckling analysis (LBA), with an amplitude of $d_c/200$. Residual stresses are not modelled. Nevertheless, the influence of a more realistic (smaller) equivalent initial imperfections is also assessed and discussed.
- Option 4: The moment resistance $M_{R,FEM}$ is obtained as the minimum of: i) the maximum value reached during analysis; ii) the moment applied at the last loading step where $\varepsilon_{pl,eq,max} \leq 5$ % (in the solid core).

Table 4
Influence of strain hardening: statistics for $M_{R,QUAD}$ / $M_{R,EPPL}$.

	Unstiffened joints (U)				Stiffened joints (T)			
n	Mean	CoV	Max	Min	Mean	CoV	Max	Min
0 %	1.04	2.0 %	1.10	1.01	1.07	3.9 %	1.15	1.01
30 %	1.03	1.4 %	1.08	1.01	1.06	3.2 %	1.12	1.00
50 %	1.02	1.0 %	1.04	1.01	1.03	2.3 %	1.08	1.00
70 %	1.01	1.0 %	1.02	0.99	1.01	1.8 %	1.05	0.98

3. Results and discussion

3.1. Influence of strain hardening and initial imperfections

The influence of the strain hardening model on the moment resistance is assessed for the one-sided internal joints, by examining the ratio $M_{R,QUAD}$ / $M_{R,EPPL}$, where $M_{R,EPPL}$ is the moment resistance obtained with the bilinear model assuming no strain hardening (EPPL), and $M_{R,QUAD}$ is the one obtained with the quad-linear model (QUAD). Eight sets are included: 1S-I-U (one-sided, internal, unstiffened) with 0 %, 30 %, 50 %, and 70 % axial load ratio, and 1S-I-T (one-sided, internal, stiffened) with 0 %, 30 %, 50 %, and 70 % axial load ratio. The statistics for this ratio are presented in Table 4 for the eight different sets considered. These statistics show that the influence of strain hardening is moderate, on average less than 4 % or 7 % for unstiffened and stiffened joints, respectively. Moreover, the influence diminishes steadily with increasing axial force.

Likewise, for the same sets (one-sided joints), the influence of the initial imperfection amplitude is assessed by examining the ratio $M_{R,420}$ / $M_{R,200}$, where $M_{R,420}$ is the moment resistance M_R obtained with an amplitude of $d_c/420$ and $M_{R,200}$ is the one obtained with an amplitude of $d_c/200$. The average of the ratio across all cases for every one of the eight sets studied is always 1.00, the CoV varies between 0.3 % and 0.7 %, the maximum is 1.03, and the minimum is 1.00, showing that the initial imperfection amplitude plays no significant role in the moment resistance of the joints examined.

Considering these results, the global assessment for the joints is carried out on the following sub-sections only for the models with no strain hardening and an imperfection amplitude of $d_c/200$.

3.2. Assessment criteria

The results of the study focus on the moment resistance M_R and the initial stiffness $S_{j,ini}$. The results are presented using the high-quality FE model as an estimate of reality, using the following ratios:

$$r_{EN} = M_{R,EN}/M_{R,FEM,5\%}, \tag{11}$$

$$r_{FprEN} = M_{R,FprEN}/M_{R,FEM,5\%}, \tag{12}$$

$$s_{EN} = S_{j,ini,EN}/S_{j,ini,FEM}, \tag{13}$$

$$s_{FprEN} = S_{j,ini,FprEN}/S_{j,ini,FEM}, \tag{14}$$

where:

- $M_{R,FEM,5\ \%}$ is the moment resistance obtained from the FE analysis at the step where the maximum equivalent plastic strain in the joint core is below or equal to 5 %, or the last step of the analysis if the 5 % equivalent plastic strain is not reached.
- $S_{j,ini,FEM}$ is the initial stiffness obtained from the FE analysis (initial step).
- $M_{R,EN}$, and $S_{j,ini,EN}$ are the moment resistance and initial stiffness, respectively, as per EN 1993–1–8:2005.
- $M_{R,FprEN}$, and $S_{j,ini,FprEN}$ are the moment resistance and initial stiffness, respectively, as per FprEN 1993–1–8:2023.

Ratios above 1 indicate that the corresponding method (EN, FprEN)

Table 5
Metrics for statistics of resistance and stiffness ratios.

Statistic	Low deviation	Intermediate deviation	High deviation
Mean	Mean < 5 %	5 % ≤ Mean < 10 %	10 % ≤ Mean
CoV	CoV < 7.5 %	7.5 % ≤ CoV < 15 %	15 % ≤ CoV

Table 6
Statistics of resistance ratios r_{method} for S275 column, one-sided, unstiffened joints (internal and roof), no axial load.

Method	Failure mode (fm)	$r_{method} = M_{R,method} / M_{R,FEM,5\ \%}$, all failure modes except BCW							
		N_{fm}	N_{fm}/N_{all}	Mean	CoV	Max	Min	(>1)	(>1)/N_{all}
Internal, unstiffened one-sided joints without axial load (1S-U-I, $n = 0$)*									
EN	All	16	100 %	0.79	13.5 %	0.95	0.60	0	0 %
	CWC	14	88 %	0.79	14.4 %	0.95	0.60	0	0 %
	CWS	2	13 %	0.80	5.6 %	0.83	0.77	0	0 %
FprEN	All	16	100 %	0.76	11.2 %	0.86	0.59	0	0 %
	CWC	14	88 %	0.75	11.6 %	0.86	0.59	0	0 %
	CWS	2	13 %	0.81	3.4 %	0.83	0.79	0	0 %
Roof, unstiffened one-sided joints without axial load (1S-U-R, $n = 0$)*									
EN	All (CWT)	20	100 %	0.69	15.7 %	0.90	0.52	0	0 %
FprEN	All (CWT)	20	100 %	0.65	13.9 %	0.79	0.50	0	0 %
Unstiffened one-sided joints without axial load (1S-U, $n = 0$)*									
EN	All	36	100 %	0.73	16.0 %	0.95	0.52	0	0 %
FprEN	All	36	100 %	0.70	14.7 %	0.86	0.50	0	0 %

* For internal joints there is no CWT failure. All roof joints fail by CWT.

yields larger results than the corresponding FE model, and in the context of this study are referred to as 'unconservative'. Correspondingly, ratios below 1 indicate that the corresponding method (EN, FprEN) gives lower results than the corresponding FE model, and in the context of this study are referred to as 'conservative'. Regarding the statistical treatment of the ratios, the metrics established in Table 5 for the mean and coefficient of variation (hereby referred to as CoV), are adopted hereinafter to facilitate the assessment.

For resistance ratios, those with BCW failure modes are excluded; however, they are considered for the initial stiffness ratios. It is further noted that the parametric study is focused on cases where the failure modes of the column web govern the bending resistance. This means that, in some cases, a higher steel grade beam had to be chosen to avoid premature beam failure. This should be considered when analysing the results and extracting conclusions on the criticality of some web panel components.

In the following sub-section, the sub-set with S275 columns is used to present and discuss the results. The assessment of the influence of steel grade is subsequently presented.

3.3. Moment resistance

3.3.1. Unstiffened one-sided joints without axial force

36 models of unstiffened one-sided joints without axial force exhibit 3 distinct failure modes: CWC, CWT, and CWS. These failure modes can be, in some cases, hardly distinguished by numerical models, and therefore, the failure modes determined by the Eurocode are shown. Table 6 lists statistics for their resistance ratios, showing that the CWT is the dominant failure mode according to the Eurocode (56 % of the cases). If the results are split according to the joint location (internal I or roof R), CWT governs the resistance of roof joints (100 % of the roof joints exhibit this failure mode) as the effective width is limited by the available column stub length above the joint. The predominant failure mode for the internal joints is CWC (88 % of cases). The ratio of the design moment resistance vs numerical resistance shows a high deviation for the mean and an intermediate deviation for the CoV. No unconservative results are obtained, with the max consistently below 1. The CWT failure mode is more conservative than the CWC. Comparing EN with FprEN, an average reduction of resistance of 3 % and a reduction of 1 % in the CoV is observed. Hence, the new design procedure does not improve results significantly and only makes them unnecessarily conservative. It should be noted that the number of results with failure of the CWS is insufficient to establish meaningful conclusions for this joint typology.

The mean of the ratio of the resistance assessed using the 5 % strain limit or the peak resistance criterion to the resistance obtained using the secant stiffness criterion (secant stiffness at 1/3 of the initial stiffness) is 99.1 %, with a CoV of 4.4 %, showing that, for this particular typology, both criteria yield very similar results.

3.3.2. Unstiffened double-sided joints without axial force

Table 7 shows the statistical results for resistance ratios, including 112 models of unstiffened double-sided joints without axial force, from which 25 exhibit CWC, 29 CWS, and 58 CWT; the latter corresponds to roof configurations, whereas CWC and CWS appear for internal configurations. The mean for both CWC and CWS failure modes with EN is very similar, (0.80 and 0.82) and shows a large deviation. The mean for CWT is slightly lower, about 0.72, also with a large CoV. Globally, there is no

Table 7
Statistics of resistance ratios r_{method} for S275 column, two-sided, unstiffened joints (internal and roof), no axial load.

Method	Failure mode (fm)	$r_{method} = M_{R,method} / M_{R,FEM,5\ \%}$, all failure modes except BCW							
		N_{fm}	N_{fm}/N_{all}	Mean	CoV	Max	Min	(>1)	(>1)/N_{all}
Internal, unstiffened two-sided joints without axial load (2S-U-I, $n = 0$)*									
EN	All	54	100 %	0.81	15.2 %	1.05	0.56	5	9 %
	CWC	25	46 %	0.80	15.1 %	1.05	0.61	2	8 %
	CWS	29	54 %	0.82	15.4 %	1.04	0.56	3	10 %
FprEN	All	54	100 %	0.83	11.3 %	1.05	0.60	2	4 %
	CWC	25	46 %	0.80	15.5 %	1.05	0.60	2	8 %
	CWS	29	54 %	0.85	5.3 %	0.92	0.73	0	0 %
Roof, unstiffened two-sided joints without axial load (2S-U-R, $n = 0$)*									
EN	All (CWT)	58	100 %	0.72	17.5 %	1.13	0.52	3	5 %
FprEN	All (CWT)	58	100 %	0.67	19.6 %	1.13	0.51	3	5 %
Unstiffened two-sided joints without axial load (2S-U, $n = 0$)*									
EN	All	112	100 %	0.77	17.2 %	1.13	0.52	8	7 %
FprEN	All	112	100 %	0.75	18.4 %	1.13	0.51	5	4 %

* For internal joints there is no CWT failure. All roof joints fail by CWT.

Table 8
Statistics of resistance ratios r_{method} for S275 column, stiffened joints, no axial load.

Method	Failure mode (fm)	$r_{method} = M_{R,method} / M_{R,FEM,5\ \%}$, all failure modes except BCW							
		N_{fm}	N_{fm}/N_{all}	Mean	CoV	Max	Min	(>1)	(>1)/N_{all}
Internal, stiffened one-sided joints without axial load (1S-T-I, $n = 0$)*									
EN	All (CWS)	14	100 %	1.00	7.6 %	1.15	0.86	8	57 %
FprEN	All (CWS)	14	100 %	0.91	3.0 %	0.96	0.86	0	0 %
Roof, stiffened one-sided joints without axial load (1S-T-R, $n = 0$)*									
EN	All (CWS)	15	100 %	0.98	7.0 %	1.14	0.91	3	20 %
FprEN	All (CWS)	15	100 %	0.90	8.5 %	1.08	0.78	1	7 %
All (internal and roof), stiffened one-sided joints without axial load (1S-T, $n = 0$)*									
EN	All (CWS)	29	100 %	0.99	7.3 %	1.15	0.86	11	38 %
FprEN	All (CWS)	29	100 %	0.91	6.4 %	1.08	0.78	1	3 %
Internal, stiffened two-sided joints without axial load (2S-T-I, $n = 0$)*									
EN	All (CWS)	41	100 %	0.93	9.3 %	1.09	0.75	8	20 %
FprEN	All (CWS)	41	100 %	0.89	2.9 %	0.96	0.84	0	0 %
Roof, stiffened two-sided joints without axial load (2S-T-R, $n = 0$)*									
EN	All (CWS)	42	100 %	0.92	8.5 %	1.10	0.83	9	21 %
FprEN	All (CWS)	42	100 %	0.89	10.5 %	1.14	0.73	5	12 %
All (internal and roof), stiffened two-sided joints without axial load (2S-T, $n = 0$)*									
EN	All (CWS)	83	100 %	0.92	8.9 %	1.10	0.75	17	20 %
FprEN	All (CWS)	83	100 %	0.89	7.7 %	1.14	0.73	5	6 %
Internal, one- and two-sided joints without axial load (T-I, $n = 0$)*									
EN	All (CWS)	55	100 %	0.95	9.5 %	1.15	0.75	16	29 %
FprEN	All (CWS)	55	100 %	0.89	3.1 %	0.96	0.84	0	0 %
Roof, one- and two-sided joints without axial load (T-R, $n = 0$)*									
EN	All (CWS)	57	100 %	0.94	8.6 %	1.14	0.83	12	21 %
FprEN	All (CWS)	57	100 %	0.89	9.9 %	1.14	0.73	6	11 %
All (internal and roof), one- and two-sided joints without axial load (T, $n = 0$)*									
EN	All (CWS)	112	100 %	0.94	9.0 %	1.15	0.75	28	25 %
FprEN	All (CWS)	112	100 %	0.89	7.4 %	1.14	0.73	6	5 %

* For stiffened joints the failure mode is always CWS.

meaningful difference between EN and FprEN (less than 2 % both for the mean and the CoV).

3.3.3. Stiffened joints without axial force

All models of stiffened joints without axial force (112 in total) exhibit CWS failure. The results, shown in Table 8, show intermediate deviation both for the mean and CoV. The EN results are better than FprEN in terms of the mean value (0.94 vs 0.89) and similar in terms of CoV (9% vs 7.4 %).

3.3.4. Effect of axial force in the column

Table 9 summarizes the results for 250 models of internal welded joints with axial force in the column varying from 0 to 70 %. The results indicate that the mean, max, and min of resistance ratio across cases increase steadily with axial force, whereas the CoV is approximately constant. Fig. 12 plots the mean of the resistance ratios for each of the four cases versus the column axial force ratio n, showing a similar increasing trend for both EN and FprEN. The mean resistance ratio for $n = 0.7$ is about 32 % higher than the mean resistance ratio for $n = 0$, regardless of joint stiffening (stiffened or unstiffened), and configuration (one- or two-sided). Individual results for one-sided joints are presented graphically in Fig. 13, showing that the trend is also present on a case-by-case basis.

Fig. 14 compares the normalized moment-rotation curves for case number 6 (column UC203 × 203 × 46 S275, beam IPE330 S235) in a one-sided internal configuration, including the 4 levels of column axial force included in the study ($n = 0$, 0.3, 0.5, 0.7). In the figure, markers are included for the last fully elastic point (marked as 'elastic'), and the moment resistance (marked as '5 % pleq'), including a label describing the region or regions where the 5 % limit is reached. In cases where instability is reached before the 5 % limit, the highest resistance obtained during analysis (last converged step) is adopted and the label reads 'end of analysis'. For comparison, additional markers are included at the points where the secant stiffness is 1/3 of the initial one ($S_{j,sec} = S_{j,ini}/3$, referred to as 'secant') and where the tangent stiffness is 1/30 of the initial one ($S_{j,tan} = S_{j,ini}/30$, referred to as 'tangent'). The reference value for secant stiffness is based on EC3–1–8 (see expression (6.28b) in the cited code), whereas the reference value for tangent stiffness has been chosen between those explored (see Fig. 11) to provide a good agreement with the reference value for secant stiffness. Fig. 14(a) refers to the unstiffened joint, whereas Fig. 14(b) shows the stiffened joint. It is observed that an increase in axial force produces a steady reduction in joint strength and rotation capacity, even for low values of axial force ($n = 0.3$). The 5 % criterion used in the study produces resistance results, which are slightly larger than those based on the 'secant' or 'tangent' criteria previously mentioned.

3.3.5. Influence of steel grade

A total of 1896 models covering steel grades S235, S275, and S355 give almost the same results, showing no dependence on steel grade, see Table 10.

3.3.6. Summary

- General trends: considering all cases in the study, EC3 and FprEC3 exhibit conservative mean results, but with a high dispersion; a large proportion of unconservative results is obtained. FprEC3 improves these results, but only marginally.
- Mean: the mean resistance ratio of all cases in the study is below 1. For cases with large axial force ($n = 0.7$), and stiffened joints (T) with axial force, the mean resistance ratio is above 1. For stiffened joints with axial load unconservative results are obtained, even for low values of n, with both EC3 and FprEC3, although less for the latter. An increase in the column axial force produces a systematic increase in the mean value, particularly for stiffened joints.
- Dispersion: considering all cases in the study, the CoV of both EC3 and FprEC3 is high, at 19.5 % (EC3) and 18.0 % (FprEC3). The dispersion is always larger for cases where the failure mode is CWC instead of those with CWS.
- Conservativeness: The proportion of unconservative cases is large, about 36 % for EC3 and 28 % for FprEC3. This proportion goes up to

Table 9
Statistics of r_{method} for S275, influence of axial load.

Method	Cases	n	$r_{method} = M_{R,method} / M_{R,FEM,5\ \%}$, all failure modes except BCW						
			N	Mean	CoV	Max	Min	(>1)	(>1)/N
EN	1S-U-I	0	16	0.79	13.5 %	0.95	0.60	0	0 %
		0.3	16	0.83	14.1 %	1.00	0.63	0	0 %
		0.5	16	0.89	14.4 %	1.07	0.68	4	25 %
		0.7	16	1.02	14.8 %	1.21	0.81	9	56 %
	1S-T-I	0	14	1.00	7.6 %	1.15	0.86	8	57 %
		0.3	14	1.06	7.5 %	1.24	0.92	11	79 %
		0.5	14	1.14	6.6 %	1.31	1.01	14	100 %
		0.7	14	1.31	8.1 %	1.51	1.18	14	100 %
	2S-U-I	0	54	0.81	15.2 %	1.05	0.56	5	9 %
		0.3	54	0.86	15.4 %	1.12	0.61	7	13 %
		0.5	54	0.92	15.1 %	1.20	0.67	14	26 %
		0.7	54	1.06	15.1 %	1.41	0.78	33	61 %
	2S-T-I	0	41	0.93	9.3 %	1.09	0.75	8	20 %
		0.3	41	0.99	9.0 %	1.17	0.81	15	37 %
		0.5	41	1.06	8.3 %	1.25	0.89	30	73 %
		0.7	41	1.20	7.7 %	1.37	1.06	41	100 %
	All I (1S, 2S, U, T)	0	125	0.87	14.7 %	1.15	0.56	21	16.8 %
		0.3	125	0.919	14.9 %	1.24	0.61	35	28.0 %
		0.5	125	0.986	14.6 %	1.31	0.67	62	49.6 %
		0.7	125	1.132	14.4 %	1.51	0.78	97	77.6 %
FprEN	1S-U-I	0	16	0.76	11.2 %	0.86	0.59	0	0 %
		0.3	16	0.79	11.7 %	0.90	0.63	0	0 %
		0.5	16	0.85	12.3 %	0.98	0.67	0	0 %
		0.7	16	0.98	13.2 %	1.17	0.78	8	50 %
	1S-T-I	0	14	0.91	3.0 %	0.96	0.86	0	0 %
		0.3	14	0.97	2.5 %	1.01	0.92	2	14 %
		0.5	14	1.03	2.7 %	1.08	1.00	11	79 %
		0.7	14	1.20	7.9 %	1.39	1.11	14	100 %
	2S-U-I	0	54	0.83	11.3 %	1.05	0.60	2	4 %
		0.3	54	0.87	11.7 %	1.10	0.62	3	6 %
		0.5	54	0.94	11.9 %	1.19	0.67	11	20 %
		0.7	54	1.09	12.8 %	1.41	0.75	42	78 %
	2S-T-I	0	41	0.89	2.9 %	0.96	0.84	0	0 %
		0.3	41	0.95	2.8 %	1.01	0.90	3	7 %
		0.5	41	1.02	2.8 %	1.08	0.97	31	76 %
		0.7	41	1.15	4.4 %	1.25	1.09	41	100 %
	All I (1S, 2S, U, T)	0	125	0.85	10.0 %	1.05	0.59	2	1.6 %
		0.3	125	0.898	10.4 %	1.10	0.62	8	6.4 %
		0.5	125	0.964	10.6 %	1.19	0.67	53	42.4 %
		0.7	125	1.107	11.4 %	1.41	0.75	105	84.0 %

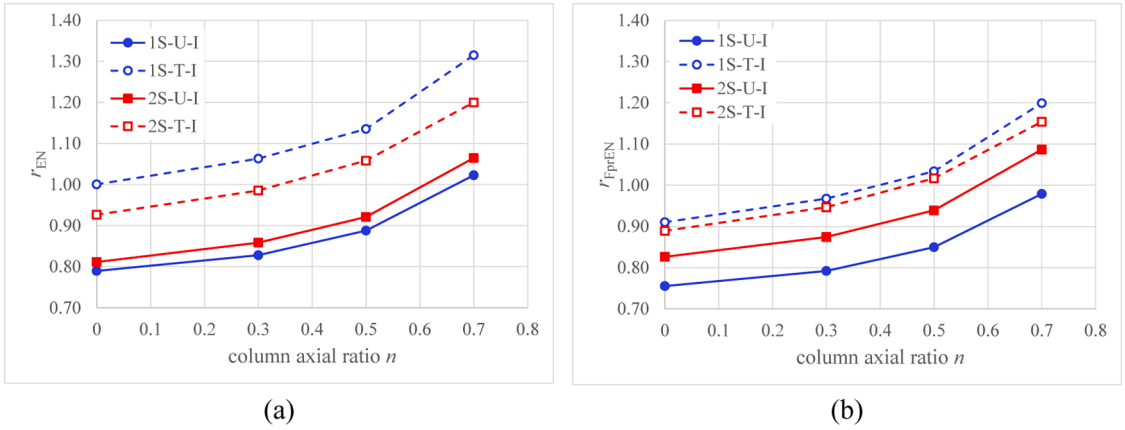

Fig. 12. Variation of mean of resistance ratio r_{method} with the level of axial force in the column n for internal joints: (a) EN; (b) FprEN.

100 % for both EC3 and FprEC3, in cases with high axial load (n = 0.7), where the minimum ratio is always above 1.

• One-sided vs two-sided joints: For EC3, the results for two-sided joints present lower mean, lower dispersion, and lower maxima, than those for one-sided joints. The minima are similar. The proportion of unconservative cases is larger for one-sided joints. For FprEC3, the results for one-sided joints present a lower mean, lower maxima, and a lower proportion of unconservative cases, although with higher dispersion.

• Internal vs roof joints: The results for roof joints present a lower mean (by about 10 %), lower minima, and lower maxima, than those for internal joints.

• Unstiffened vs stiffened joints: The results for unstiffened joints present a lower mean, lower maxima, and lower minima than those

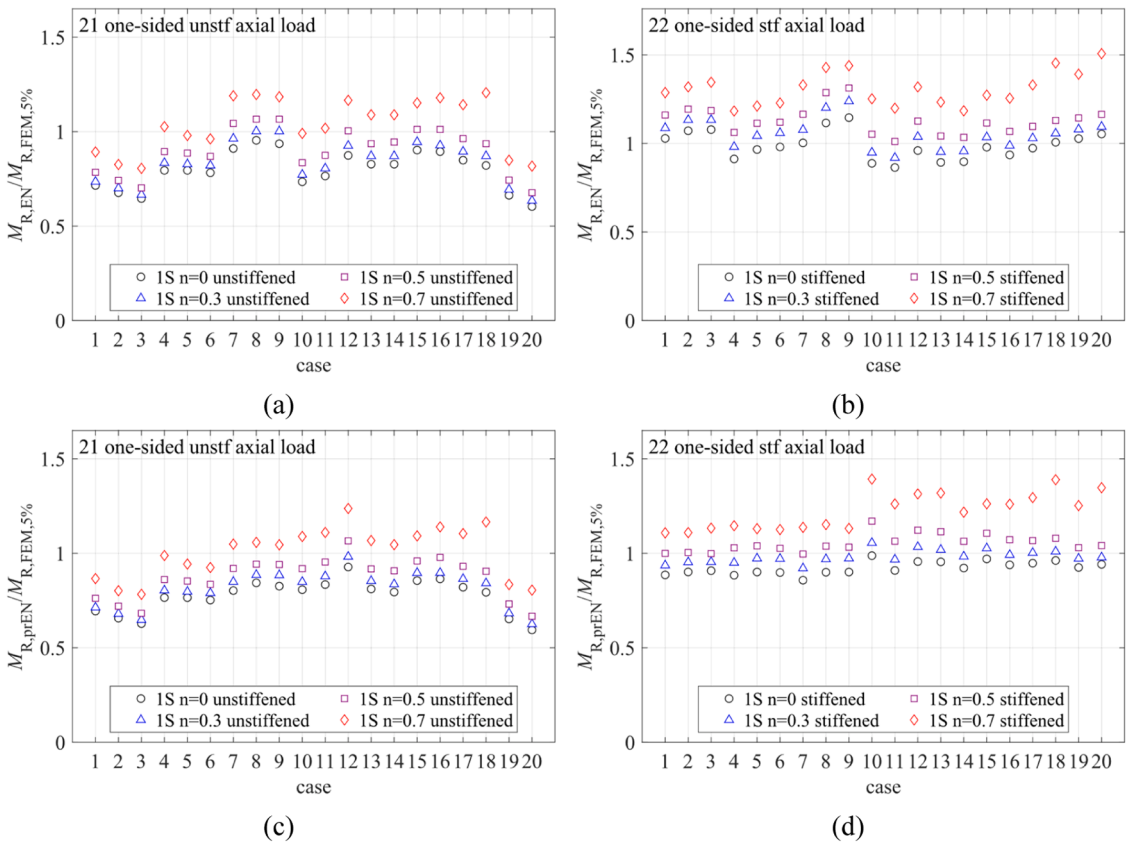

Fig. 13. Influence of axial load on resistance ratio r_{method} across cases: (a) EN, unstiffened joints; (b) EN, stiffened joints; (c) FprEN, unstiffened joints; (d) FprEN, stiffened joints.

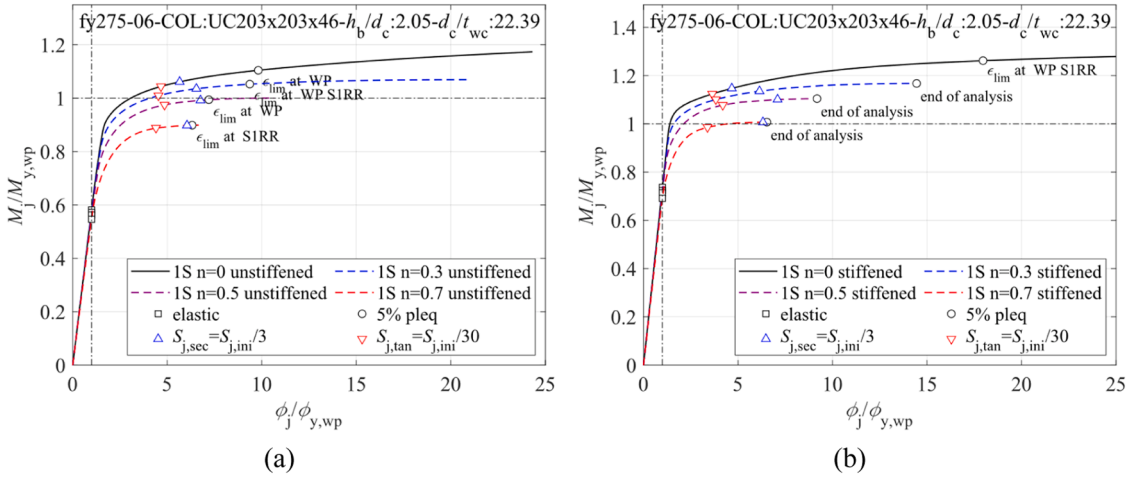

Fig. 14. Influence of axial load in the moment-rotation curves for case 6, one-sided, internal: (a) unstiffened joint; (b) stiffened joint.

for stiffened joints, but with a larger dispersion. The proportion of unconservative cases is much larger for stiffened joints.

- Effect of axial force: Inclusion of axial load, even below the 70 % threshold, results in unconservative results for both EC3 and FprEC3, particularly for stiffened joints. Increasing values of axial load result in higher mean, larger dispersion, larger maximum and minimum values, and a larger proportion of unconservative cases, for both codes.
- Failure modes: the CWS component is the most unconservative, with a higher mean and a larger proportion of cases with ratios over 1 (48 % and a maximum of 1.51 for EC3, 36 % and a maximum of 1.39 for FprEC3). The CWC and CWT components are affected by the level of axial load, but for the CWC this effect is small. The CWS component is sensitive to the level of axial load, with substantial increases in mean, maximum, minimum, and proportion of unconservative results when the cases with $n = 0$ and $n = 0.7$ are compared.
- Web panel slenderness: there is no clear influence of the web panel slenderness on these results.

3.4. Initial stiffness

Statistics for the stiffness ratios for all (2400) models of welded joints

Table 10
Statistics of resistance ratios r_{method} for different steel grades (all sets included).

Method	Steel grade	$r_{method} = M_{R,method} / M_{R,FEM,5\ \%}$, all failure modes except BCW						
		N	Mean	CoV	Max	Min	(>1)	(>1)/ *N*
EN	ALL	1896	0.94	19.6 %	1.58	0.51	696	37 %
	S235	635	0.94	19.0 %	1.47	0.51	230	36 %
	S275	635	0.94	19.5 %	1.51	0.52	230	36 %
	S355	626	0.94	20.4 %	1.58	0.54	236	38 %
FprEN	ALL	1896	0.91	18.2 %	1.46	0.49	535	28 %
	S235	635	0.91	17.6 %	1.39	0.49	173	27 %
	S275	635	0.91	18.0 %	1.41	0.50	177	28 %
	S355	626	0.91	18.8 %	1.46	0.52	185	30 %

Table 11
Statistics of stiffness ratios s_{method} (including all steel grades).

Method	Sets	$s_{method} = S_{j,ini,method} / S_{j,ini,FEM}$						
		N	Mean	CoV	Max	Min	(>1)	(>1)/ *N*
EN	All	2400	1.53	82.3 %	8.15	0.45	1323	55 %
	1S-U, $n = 0$	120	0.95	20.2 %	1.42	0.61	48	40 %
	1S-T, $n = 0$	120	1.81	16.1 %	2.42	1.43	120	100 %
	2S-U, $n = 0$	360	0.83	33.7 %	1.81	0.45	81	23 %
	2S-T, $n = 0$	360	2.14	83.4 %	6.33	0.57	198	55 %
	U, $n > 0$	720	1.02	28.5 %	2.27	0.50	358	50 %
	T, $n > 0$	720	2.15	72.6 %	8.15	0.58	518	72 %
FprEN	All	2400	1.32	78.9 %	7.06	0.41	1063	44 %
	1S-U, $n = 0$	120	0.89	19.1 %	1.30	0.59	27	23 %
	1S-T, $n = 0$	120	1.52	16.1 %	2.20	1.20	120	100 %
	2S-U, $n = 0$	360	0.77	37.0 %	1.74	0.41	63	18 %
	2S-T, $n = 0$	360	1.79	83.6 %	5.38	0.49	150	42 %
	U, $n > 0$	720	0.94	30.5 %	2.10	0.44	276	38 %
	T, $n > 0$	720	1.80	72.6 %	7.06	0.50	427	59 %

are included in Table 11. The results are also split by joint configuration, with and without axial load. Concerning stiffness, deviations from a mean of 1.0 lead to different internal forces in the column, beam, and joint. The results show a good agreement for the unstiffened cases. However, for the stiffened cases, the average results vary from 1.52 to 2.14. Considering all cases in the study, the mean value of the stiffness ratio is above 1. It can be up to 1.53 (EC3) or 1.32 (FprEC3). It is systematically closer to the FEM results for FprEC3, but still high. Moreover, the scatter is high (82 % in EC3 and 79 % in FprEC3). This is consistently found for all types of joints, except unstiffened joints, which feature much better results (mean below 1, lower dispersion, lower maxima). Axial load application results in more conservative results.

4. Conclusions

This paper reports on a large study conducted at the University of Coimbra to assess the design rules for welded steel beam-to-column joints for open sections, covering joint position (internal story or roof), configuration (one- or two-sided), stiffening (without or with transverse stiffeners), applied column axial load and the ratio of applied moment between both sides and three steel grades, totalling 2400 joints. The study is focused on moment resistance and initial stiffness obtained using the current EC3 and its forthcoming revision FprEC3.

The following conclusions could be reached:

- The resistance ratios for both codes (EC3 and FprEC3) present an average close to 1, with a high scatter, and are, for a remarkably large proportion of cases, higher than 1. Deviations are particularly large for stiffened joints with axial force, suggesting that the formulation of the column components (particularly web panel in shear) should be revised for cases with column axial force, even for low values of the latter.
- The stiffness ratios for both codes present an average larger than 1, with a remarkably large scatter, and very large maxima. Although it is well known that the initial stiffness is very sensitive to small variations, the results for stiffened joints are much worse than for unstiffened joints, suggesting that the contribution of stiffeners should be considered more carefully when assessing joint stiffness.
- The forthcoming FprEC3 provides only a marginal improvement in these results. The improvement is slightly larger for stiffness than for resistance.
- The results show that the EC3 procedure predicts unconservative results for stiffened joints with axial force. Because the dominant failure mode in these joints is CWS, it seems that the formulation of this component needs improvement to consider the influence of the axial load. The FprEC3 procedure improves these results but only marginally, to the cost of a general reduction of resistance (with or without axial force). The web panel is the controlling element for the joint distortion, and the code formulation does not consider the rapid yielding of the web panel in the shear component when axial force is present.

The study presents some limitations. Due to the large scale of the sample, the FE models could not include a sophisticated model for welds; instead, continuity is assumed between the beam and column. The material model is elastic-perfectly-plastic, so the moment resistance results do not include any effect of strain hardening, although it was shown that the impact of strain hardening leads to an average increase of the moment resistance of about 5 %. Material damage is not included. Residual stresses are indirectly considered through an equivalent initial imperfection. Finally, no reliability assessment was carried out, therefore no objective statements can be made about the compliance with the safety requirements of the structural Eurocodes.

As a conclusion, this assessment highlights the need to revisit the formulations for the column web panel, especially as bolted joints have deserved much less attention, and the need to carry out a systematic reliability assessment to ensure that the target probability of failure is met.

CRediT authorship contribution statement

Jorge Conde: Conceptualization, Methodology, Software, Validation, Formal analysis, Writing – original draft, Writing – review & editing. **Fernando Freire:** Writing – review & editing, Writing – original draft, Validation, Software, Methodology, Investigation, Formal analysis. **Filip Ljubinković:** Writing – review & editing, Writing – original draft, Methodology, Conceptualization. **Martin Vild:** Writing – review & editing, Conceptualization. **Luís Simões da Silva:** Writing – review & editing, Writing – original draft, Supervision, Methodology,

Conceptualization.

Declaration of competing interest

The authors declare that they have no known competing financial interests or personal relationships that could have appeared to influence the work reported in this paper.

Data availability

Data will be made available on request.

Acknowledgment and funding sources

This work was partly financed by:

- FCT / MCTES through national funds (PIDDAC) under the R&D Unit Institute for Sustainability and Innovation in Engineering Structures (ISISE), under reference UIDB / 04029/2020, and under the Associate Laboratory for Advanced Manufacturing and Intelligent Systems (ARISE) under reference LA/P/0112/2020.
- Grant with reference UP2021–035 (RD 289/2021) from "Ministerio de Universidades de España", funded by European Union, NextGenerationEU, attributed to Jorge Conde.
- Grant with reference 2021.05912.BD attributed to Fernando Freire Ribeiro, funded by FCT - Foundation for Science and Technology, Portugal.
- Idea StatiCa through Research Contract 2023_250401.

ANNEX. A: summary of Eurocode expressions

The expressions of EC3–1–8 for verification of welded beam-column joints are based on the Component Method (CM). The method is based on the identification of the joint active components, subsequent assessment of their individual structural properties, and creation of a joint model assembling the individual components by means of rigid links and springs. Fig. A1 shows the CM model for the joints analysed in this paper. Fig. A1(a) displays the joint geometry, and Fig. A1(b) the corresponding component model. The one-sided joint is modelled with a top and bottom part, aligned with the centroid of the corresponding beam flange; every part is formed by a series of line springs with only one degree of freedom (they cannot elongate or displace out of their line of action) joined with rigid links. A rotational spring is added to represent the BCW component. The line springs have a translational degree of freedom and the rotational spring has a rotational degree of freedom. The links have infinite resistance and stiffness, whereas the springs have a limited resistance, and may have finite or infinite stiffness. The expressions to calculate the component's resistance and stiffness are listed in Table A1 for both the current EC3–1–8 and the upcoming FprEC3–1–8. Notice that for components CWS, CWC, CWT, CFB, the moment resistance expressions contain the lever arm z_b, so dividing by this value the component resistance in terms of force is obtained and can be assigned to the corresponding springs. This is not the case for the BCW component, which is added as a rotational spring to the model. The moment resistance of the assembly can be found using Eq. (1). The stiffness values in Table A1 correspond to the line springs and are normalized (as usual) by the Young Modulus of steel E. The rotational stiffness of the assembly can be obtained using Eq. (2).

Table A1
Summary of expressions in EC3–1–8 and FprEC3–1–8.

	EC3–1–8	FprEC3–1–8
Conditions in this study	One- or double-sided joints, hot-rolled open sections (H, I), strong-axis, welded connections. With or without transverse stiffeners. For double-sided joints, equal beam height. For stiffened joints, transverse stiffeners in both tension and compression zones, aligned with beam flanges, $f_{yst}=f_{yb}$, $t_{st}=t_{fb}$, $b_{st}=b_{fb}$.	
Limits	$d_c/t_{wc} \le 69\sqrt{235\text{MPa}/f_{yc}}$	$h_c/t_{wc} \le 60\sqrt{235\text{MPa}/f_{yc}}$
CWS	**Resistance**: $M_{CWS,Rd,side} = z_b V_{wp,tot,Rd}/\beta_{side}$,	
	$V_{wp,tot,Rd} = V_{wp,Rd} + V_{wp,add,Rd}$, $V_{wp,Rd} = 0.9A_{CWS}f_{yc}/\gamma_{M0}\sqrt{3}$	
	$z_b = h_b - t_{fb}$, $\beta_1 = \lvert 1 - M_{j,b2,Ed}/M_{j,b1,Ed}\rvert \le 2$, $\beta_2 = \lvert 1 - M_{j,b1,Ed}/M_{j,b2,Ed}\rvert \le 2$	
	$A_{CWS} = A - 2bt_{fc} + (t_{wc} + 2r_c)t_{fc}$	$A_{CWS} = h_c t_{wc}$
	Unstiffened joint: $V_{wp,add,Rd} = 0$	Unstiffened joint: $V_{wp,add,Rd} = 4M_{pl,fc,Rd}/z_b$,
	Stiffened joint: $V_{wp,add,Rd} = 4M_{pl,fc,Rd}/z_b$	Stiffened joint: $V_{wp,add,Rd} = (4M_{pl,fc,Rd} + 2n_c M_{pl,fb,Rd})/z_b$
	$n_c = 1$ (one-sided) or 2 (double-sided), $M_{pl,fb,Rd} = 0.25 b_{fb} t_{fb}^2 f_{yb}$, $M_{pl,fc,Rd} = 0.25 b_{fc} t_{fc}^2 f_{yc}$	
	Stiffness: $k_{CWS} = 0.38A_{CWS}/(\beta z_b)$	
CWT	**CWT Resistance:** $M_{CWT,Rd} = z_b\, \omega\, b_{eff,CWT} t_{wc} f_{yc}/\gamma_{M0}$	
CWC	**CWC Resistance:** $M_{CWC,Rd} = z_b \min\{\rho\, \omega\, k_{wc}\, b_{eff,CWC} t_{wc} f_{yc}/\gamma_{M1}; \omega\, k_{wc}\, b_{eff,CWC} t_{wc} f_{yc}/\gamma_{M0}\}$	
	Internal: $b_{eff,CWT} = t_{fb} + 2\sqrt{2}a_b + 5(t_{fc} + r_c)$.	
	Roof: $b_{eff,CWT} = t_{fb} + \sqrt{2}a_b + 2.5(t_{fc} + r_c)$	
	$b_{eff,CWC} = t_{fb} + 2\sqrt{2}a_b + 5(t_{fc} + r_c)$, $k_{wc} = \begin{cases} \sigma_{com,Ed} \le 0.7f_{yc} & \rightarrow k_{wc} = 1 \\ \sigma_{com,Ed} > 0.7f_{yc} & \rightarrow k_{wc} = 1.7 - \sigma_{com,Ed}/f_{yc} \end{cases}$	
	$\begin{cases} 0 \le \beta \le 0.5, & \rightarrow \omega = 1, \\ 0.5 < \beta < 1, & \rightarrow \omega = \omega_1 + 2(1-\beta)(1-\omega_1), \\ \beta = 1, & \rightarrow \omega = \omega_1, \\ 1 < \beta < 2, & \rightarrow \omega = \omega_1 + (\beta - 1)(\omega_2 - \omega_1), \\ \beta = 2, & \rightarrow \omega = \omega_2. \end{cases}$ with $\begin{cases} \omega_1 = \dfrac{1}{\sqrt{1 + 1.3(b_{eff,CWT} t_{wc}/A_{CWS})^2}} \\ \omega_2 = \dfrac{1}{\sqrt{1 + 5.2(b_{eff,CWT} t_{wc}/A_{CWS})^2}}, \end{cases}$	
	$\overline{\lambda}_p = 0.932\sqrt{\dfrac{b_{eff,CWC}\, d_{wc}\, f_{yc}}{E t_{wc}^2}}$	$\overline{\lambda}_p = 0.932\sqrt{\dfrac{\omega k_{wc} b_{eff,CWC}\, d_{wc}\, f_{yc}}{E t_{wc}^2}}$
	$\begin{cases} \overline{\lambda}_p \le 0.72 & \rightarrow \rho = 1 \\ \overline{\lambda}_p > 0.72 & \rightarrow \rho = (\overline{\lambda}_p - 0.2)/\overline{\lambda}_p^2 \end{cases}$	$\begin{cases} \overline{\lambda}_p \le 0.673 & \rightarrow \rho = 1 \\ \overline{\lambda}_p > 0.673 & \rightarrow \rho = (\overline{\lambda}_p - 0.22)/\overline{\lambda}_p^2 \end{cases}$
	Stiffness: unstiffened joints $k_{CWC} = 0.7 b_{eff,CWC} t_{wc}/d_{wc}$, $k_{CWT} = 0.7 b_{eff,CWT} t_{wc}/d_{wc}$ stiffened joints, $k_{CWC} = k_{CWT} = \infty$.	

(continued on next page)

Table A1 (*continued*)

	EC3–1–8 FprEC3–1–8
CFB	Joint needs stiffeners if $b_{eff} \geq b_b f_{yb}/f_{ub}$ **Resistance:** (only for unstiffened joints): $M_{CFB,Rd} = z_b\, b_{eff}\, t_{fb} f_{yb}/\gamma_{M0}$ $b_{eff} = t_{wc} + 2r_c + 7k\, t_{fb}$, $k = t_{fc} f_{yc}/(t_{fb} f_{yb}) \leq 1$. **Stiffness:** ∞
BCW	**Resistance** (full penetration butt welds): $M_{BCW,Rd} = W_{pl,b} f_{w,Rd}$, $W_{pl,b}$ is the strong-axis plastic modulus of the beam footprint on the column, $f_{w,Rd} = \min\{f_{yc}, f_{yb}\}/\gamma_{M0}$ **Stiffness:** ∞

NOTE: Symbols defined in the 'Notation' section.

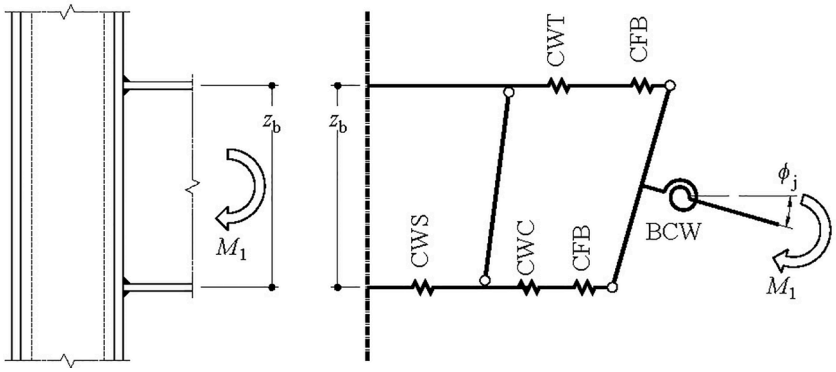

Fig. A1. Component Method: (a) actual joint; (b) CM spring and link model.

ANNEX. B: constitutive laws

This Section summarizes the constitutive laws used in the FE analysis. As mentioned in the main text, two materials are considered: (i) an elastic-perfectly plastic material (EPPL) with no strain hardening; and (ii) the quad-linear material model (QUAD) developed by Yun and Gardner [26] that considers strain hardening. For the EPPL material, the engineering stress σ_{EPPL} as a function of engineering strain ε is given by:

$$\sigma_{EPPL} = \begin{cases} E\varepsilon & \text{for } \varepsilon \leq \varepsilon_{y,} \\ f_y & \text{for } \varepsilon_y < \varepsilon; \end{cases} \tag{B.1}$$

where f_y is the material's yield stress, E is the material's Young Modulus, and ε_y is the strain at the yield point obtained as f_y/E. Nominal properties were used. For the QUAD material, the engineering stress is given by:

$$\sigma_{QUAD} = \begin{cases} E\varepsilon & \text{for } \varepsilon \leq \varepsilon_y, \\ f_y & \text{for } \varepsilon_y < \varepsilon \leq \varepsilon_{sh}, \\ f_y + E_{sh}(\varepsilon - \varepsilon_{sh}) & \text{for } \varepsilon_{sh} < \varepsilon \leq C_1\varepsilon_u, \\ f_{C_1\varepsilon_u} + \dfrac{f_u - f_{C_1\varepsilon_u}}{\varepsilon_u - C_1\varepsilon_u}(\varepsilon - C_1\varepsilon_u) & \text{for } C_1\varepsilon_u < \varepsilon \leq \varepsilon_u; \end{cases} \tag{B.2}$$

$$\varepsilon_u = 0.6\left(1 - f_y / f_u\right) \geq 0.06, \tag{B.3}$$

$$\varepsilon_{sh} = \min\left\{0.1 f_y / f_u - 0.055; 0.03\right\} \geq 0.015, \tag{B.4}$$

$$C_1 = \frac{\varepsilon_{sh} + 0.25(\varepsilon_u - \varepsilon_{sh})}{\varepsilon_u}, \tag{B.5}$$

$$E_{sh} = \frac{f_u - f_y}{0.4(\varepsilon_u - \varepsilon_{sh})}, \tag{B.6}$$

$$f_{C_1\varepsilon_u} = f_y + E_{sh}(C_1\varepsilon_u - \varepsilon_{sh}), \tag{B.7}$$

where f_u is the material's tensile strength. The engineering stress σ and strain ε were further converted to true stress σ_T and true strain ε_T prior to introduction in the FE program, using the well-known expressions:

$$\sigma_T = \sigma(1 + \varepsilon), \tag{B.8}$$

$$\varepsilon_T = \ln(1 + \varepsilon), \tag{B.9}$$

The stress-strain curves of the material models defined are plotted in Fig. B1 for S275

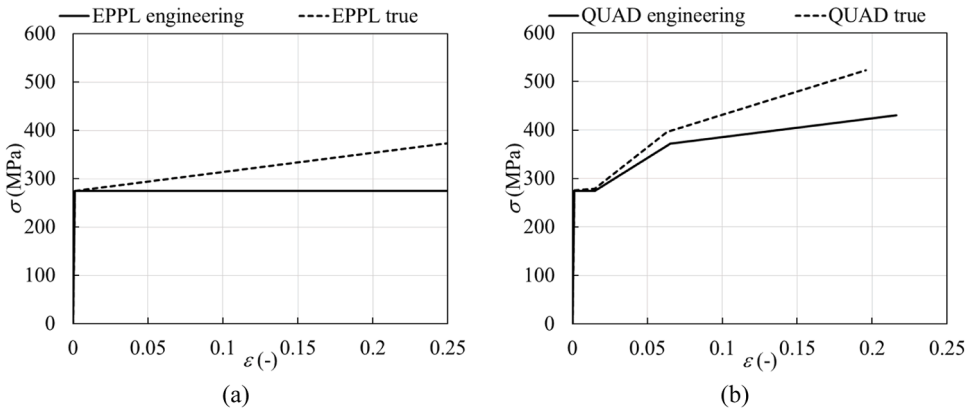

Fig. B1. Stress-strain curves of the material models considered for S275: (a) Elastic-perfectly plastic (EPPL); (b) Quad-linear (QUAD).

References

[1] J.P. Jaspart and K. Weynand, Design of joints in steel and composite structures. ECCS and Ernst & Sohn, Wiley, Brussels, Belgium, 2016.

[2] L. Simões da Silva, et al., Experimental behaviour of large-size beam-to-column steel joints for the DUNE neutrino experiment, Thin-Walled Struct. 191 (2023) 110996, https://doi.org/10.1016/j.tws.2023.110996.

[3] S. Jordão, L. Simões da Silva, R. Simões, Behaviour of welded beam-to-column joints with beams of unequal depth, J. Constr. Steel Res. 91 (2013) 42–59, https://doi.org/10.1016/j.jcsr.2013.07.023.

[4] J. Parfitt and W.F. Chen, "Tests of welded steel beam-to-column moment connections," Bethlehem, 1974.

[5] S.K. Bose, G.M. McNeice, A.N. Sherbourne, Column webs in steel beam-to-column connexions part I—Formulation and verification, Comput. Struct. 2 (1) (1972) 253–279, https://doi.org/10.1016/0045-7949(72)90030-2.

[6] H. Tanaka, Proposal of design formulae for required web-thickness of beam-column connections, Archit. Inst. Jpn. 207 (1973) 19–26, https://doi.org/10.3130/aijsaxx.207.0_19, 72.

[7] H. Krawinkler, V.V. Bertero, E.P. Popov, Shear behavior of steel frame joints, J. Struct. Div. 101 (11) (1975) 2317–2336, https://doi.org/10.1061/jsdeag.0004206.

[8] American institute of steel construction, ANSI/AISC 360-22 - specification for structural steel buildings. United States of America, 2022. [Online]. Available: https://www.aisc.org/publications/steel-standards/aisc-360/.

[9] P. Zoetemeijer, "The influence of normal, bending and shear stresses on the ultimate compression force exerted laterally to European rolled sections (in Dutch) - Stevin Laboratory: steel structures, Report 6-75-18," The Netherlands, 1975.

[10] F. Tschemmernegg, C. Humer, The design of structural steel frames under consideration of the nonlinear behaviour of joints, J. Constr. Steel Res. 11 (2) (1988) 73–103, https://doi.org/10.1016/0143-974x(88)90045-4.

[11] W.S. Atamaz and F. Frey, "Numerical simulation of the behaviour of connections," Workshop on connections and the behaviour, strength and design of steel structures, 1987.

[12] J.P. Jaspart, "Etude de la semi-rigidité des noeuds poutre-colonne et son influence sur la résistance et la stabilité des ossatures en acier", PhD Thesis, Université de Liège, 1991. http://hdl.handle.net/2268/30426.

[13] W.S. Atamaz and J.P. Jaspart, "Étude du comportement jusqu'a la ruine des noeuds complètement soudés - Rapport Interne IREM 89/7," 1989.

[14] J.P. Jaspart, "Recent advances in the field of steel joints - column bases and further configurations for beam-to-column joints and beam splices," Aggregate thesis, University of Liège, 1997.

[15] CEN, EN 1993-1-8 - Eurocode 3: Design of Steel Structures - Part 1-8: Design of Joints, European Committee for Standardization, Belgium, 2005, p. 135.

[16] S. Jordão, L. Simões da Silva, R. Simões, Design formulation analysis for high strength steel welded beam-to-column joints, Eng. Struct. 70 (2014) 63–81, https://doi.org/10.1016/j.engstruct.2014.02.028.

[17] A.M. Girão Coelho, F.S.K. Bijlaard, H. Kolstein, Experimental behaviour of high-strength steel web shear panels, Eng. Struct. 31 (7) (2009) 1543–1555, https://doi.org/10.1016/j.engstruct.2009.02.023.

[18] A. Corman, "Characterization of the Full Non-Linear Behaviour up to Failure of the Sheared Panel Zone under Monotonic Loading Conditions," 2022. [Online]. Available: https://orbi.uliege.be/bitstream/2268/295738/1/THESIS_AC_final_proof.pdf.

[19] A. Corman, J. Jaspart, J. Demonceau, Resistance of the beam-to-column component "column web panel in shear, Steel Constr. 12 (3) (2019) 222–230, https://doi.org/10.1002/stco.201900020.

[20] A. Corman, J.F. Demonceau, J.P. Jaspart, Analytical model for the panel zone resistance in welded steel beam-to-column joints, J. Constr. Steel Res. 189 (107099) (2022), https://doi.org/10.1016/j.jcsr.2021.107099.

[21] J.P. Jaspart, A. Corman, J.F. Demonceau, Characterization of unstiffened column webs in transverse compression in steel beam-to-column joints, Thin-Walled Struct. 180 (109848) (2022), https://doi.org/10.1016/j.tws.2022.109848.

[22] CEN, FprEN 1993-1-8 - Eurocode 3: design of steel structures - Part 1-8: joints. Belgium: European Committee for Standardization, 2022, p. 214.

[23] CEN, prEN 1993-1-14: design of steel structures - Part 1-14: design assisted by finite element analysis, no. January. Belgium: European Committee for Standardization, 2022, p. 61.

[24] L. Simões da Silva, Towards a consistent design approach for steel joints under generalized loading, J. Constr. Steel Res. 64 (9) (2008) 1059–1075, https://doi.org/10.1016/j.jcsr.2008.02.017.

[25] Simulia, "Abaqus user Manual [online]," Dassault Systèmes R2022x User Assistance, 2022. [Online]. Available: https://help.3ds.com/HelpProductsDS.aspx.

[26] X. Yun, L. Gardner, Stress-strain curves for hot-rolled steels, J. Constr. Steel Res. 133 (2017) 36–46, https://doi.org/10.1016/j.jcsr.2017.01.024.

[27] B. Johansson, R. Maquoi, G. Sedlacek, C. Müller, and D. Beg, "Commentary and worked examples to EN 1993-1-5 'plated structural elements,'" Luxembourg, 2007. [Online]. Available: https://publications.jrc.ec.europa.eu/repository/handle/JRC38239.

[28] G.R. Johnson, W.H. Cook, A constitutive model and data for metals subjected to large strains, high strain rates and high temperatures, in: Proceedings of the 7th International Symposium on Ballistics, The Hague, 1983, pp. 541–547.

[29] H. Klein, "Das elastisch-plastische Last-Verformungsverhalten M-v steifenloser, geschweisster Knoten für die Berechnung von Stahlrahmen mit HEB-Stützen (in German)," 1985.

[30] S. Jordão, "Comportamento de juntas soldadas em nó interno com vigas de diferentes alturas e aço de alta resistência (in Portuguese)," 2008. [Online]. Available: http://hdl.handle.net/10316/7542.